ACS APPLIED MATERIALS & INTERFACES

Research Article

Cite This: ACS Appl. Mater. Interfaces XXXX, XXX, XXX−XXX

www.acsami.org

# Disulfiram Copper Nanoparticles Prepared with a Stabilized Metal Ion Ligand Complex Method for Treating Drug-Resistant Prostate Cancers

Wu Chen,[†] Wen Yang,[‡] Pengyu Chen,[‡] Yongzhuo Huang,[*,§] and Feng Li[*,†]

[†]Department of Drug Discovery and Development, Harrison School of Pharmacy, and [‡]Materials Research and Education Center, Materials Engineering, Department of Mechanical Engineering, Auburn University, Auburn, Alabama 36849, United States

[§]State Key Laboratory of Drug Research, Shanghai Institute of Materia Medica, Chinese Academy of Sciences, Shanghai 201203, China

Supporting Information

**ABSTRACT:** Disulfiram (DSF), an alcohol-aversion drug, has been explored for cancer treatment. Copper diethyldithiocarbamate ($Cu(DDC)_2$) complex formed by DSF and copper ions is a major active ingredient for its anticancer activity. Direct administration of $Cu(DDC)_2$ is a promising strategy to enhance the anticancer efficacy of DSF. However, efficient drug delivery remains a significant challenge for $Cu(DDC)_2$ and hinders its clinical use. In this study, we developed a facile stabilized metal ion ligand complex (SMILE) method to prepare $Cu(DDC)_2$ nanoparticles (NPs). The SMILE method could prepare $Cu(DDC)_2$ NPs with different types of stabilizers including 1,2-distearoyl-*sn*-glycerol-3-phosphoethanolamine−poly(ethylene glycol) (PEG) 2000, D-*α*-tocopherol PEG 1000 succinate, methoxy PEG 5000-*b*-poly(L-lactide) 5000, and other generally recognized as safe excipients approved by the US Food and Drug Administration. The optimized formulations demonstrated excellent drug-loading efficiency (close to 100%), high drug concentrations (increased drug concentration by over 200-fold compared to the traditional micelle formulation), and an optimal particle size in the sub-100 nm range. $Cu(DDC)_2$ NPs exhibited outstanding stability in serum for 72 h and can also be stored at room temperature for at least 1 month. The anticancer effects of $Cu(DDC)_2$ NP formulations were determined by multiple assays including 3-(4,5-dimethyl-thiazol-2-yl)-2,5-diphenyl tetrazolium bromide assay, colony-forming assay, calcein-AM/propidium iodide staining, and others. $Cu(DDC)_2$ NPs showed excellent activity against drug-resistant prostate cancer cells and other cancer cells with a half-maximal inhibitory concentration ($IC_{50}$) of around 100 nM. Our study also demonstrated that $Cu(DDC)_2$ NPs induced cell death in drug-resistant prostate cancer cells (DU145-TXR) through paraptosis, which is a nonapoptotic cell death. To our best knowledge, the SMILE method provides, for the first time, a simple yet efficient process for generating $Cu(DDC)_2$ NPs with high drug concentration, excellent loading efficiency, and desirable physicochemical properties. This method could potentially address drug delivery challenges of DSF/copper-based chemotherapy and facilitate its clinical translation.

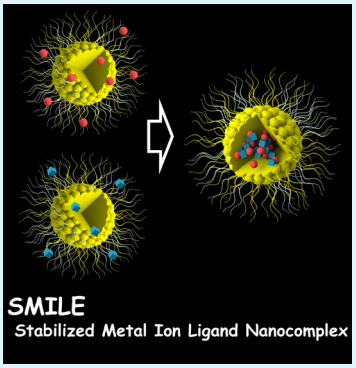


**KEYWORDS:** *disulfiram, copper diethyldithiocarbamate, drug resistance, prostate cancer, nanoparticle, drug delivery, paraptosis*



## 1. INTRODUCTION

Prostate cancer is the most common male cancer in America; about one man in nine will have prostate cancer. Prostate cancer is also the second leading cause of cancer-associated death among males in the USA (https://www.cancer.org/cancer/prostate-cancer/about/key-statistics.html). Although multiple therapeutic strategies, such as hormone therapy and radiation, have been used successfully for early-stage prostate cancer, it inevitably progresses to an aggressive form of castration-resistant prostate cancer (CRPC). Although early-stage localized prostate cancer can be effectively treated with less difficulty, the treatment of late-stage aggressive and metastatic forms of prostate cancer presents a significant challenge. Chemotherapy with taxanes is often used as a first-line drug when prostate cancer has migrated outside the prostate gland and becomes resistant to hormone therapy.[1,2] However, taxane therapy failed to show good responses in half of the patients. Even for patients with good initial responses, they may eventually develop drug-resistant prostate cancer.[2−6] Because of the lack of effective therapy, patients with drug-resistant prostate cancer have a very poor prognosis. Both the private sector and academia have put forth substantial efforts to develop new therapies for drug-resistant prostate cancer. New drugs, such as ixabepilone and cabazitaxel, have been developed for treating refractory cancer. However, the development of a new drug molecule usually takes a long time and requires significant investment, which eventually results in a high cost of the treatment. Therefore, the

Received: August 31, 2018
Accepted: October 30, 2018




DOI: 10.1021/acsami.8b14940
ACS Appl. Mater. Interfaces XXXX, XXX, XXX−XXX

**Scheme 1. Preparation of $Cu(DDC)_2$ NPs with the SMILE Method**

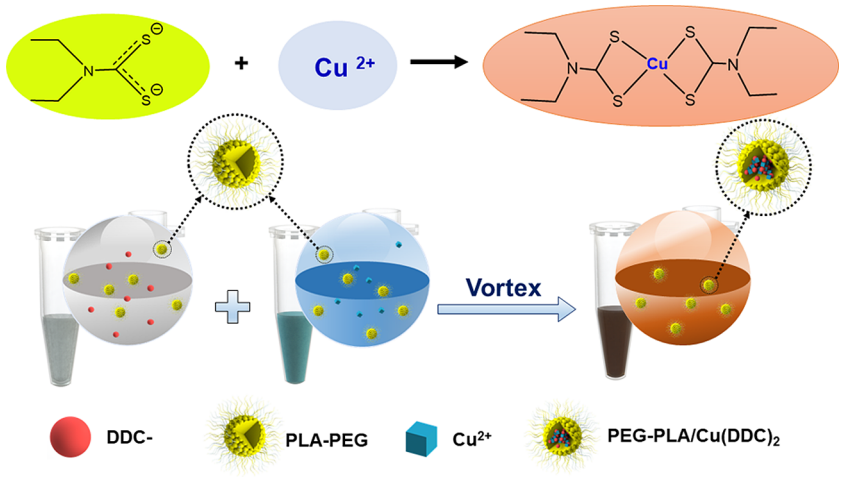


development of effective but more affordable therapeutic agents for drug-resistant prostate cancer will greatly benefit patients with this disease. Particularly, it will help those patients with financial constraints, which limit their access to oncology drugs affixed with skyrocketing prices.

Drug repurposing or repositioning has received increasing attention as an alternative strategy for drug discovery and development.[7] Disulfiram (DSF) is an alcohol-aversion drug used for treating alcohol dependence for over 60 years. Recently, DSF has been repurposed as an anticancer agent and shows excellent anticancer activity when it is combined with copper ions ($Cu^{2+}$).[8,9] DSF/Cu has been shown to inhibit the proteasome/poly-Ub protein degradation pathway by targeting the nuclear protein localization 4 (NPL4) protein.[9,10] DSF/Cu could also inhibit cancer stem cells[11,12] and sensitize resistant cancer to chemotherapy drugs by inhibiting P-gp.[13] Several ongoing clinical trials are testing the DSF/copper combination in patients with glioblastoma and metastatic CRPC.[14] The drug repurposing strategy will expedite the drug development process and facilitate the clinical translation.[15] The anticancer activity of DSF/copper is greatly dependent on the formation of the active metabolite, copper diethyldithiocarbamate ($Cu(DDC)_2$).[10] Because of the poor in vivo stability and rapid degradation of DSF,[9,11] the coadministration of DSF and copper to patients yielded extremely low in vivo concentrations of $Cu(DDC)_2$, which would significantly compromise the anticancer efficacy and result in poor clinical outcomes. Thus, the administration of the preformed $Cu(DDC)_2$ complex is expected to be a more effective approach to obtain higher active drug concentrations and to achieve better anticancer efficacy.[16]

Because of the low water solubility of $Cu(DDC)_2$, there is a great need to develop a formulation designed to increase $Cu(DDC)_2$ solubility, thereby making it acceptable for clinical use.[16,17] Nanotechnology-based approaches have been used for the delivery of $Cu(DDC)_2$.[16,18,19] In previous studies, the direct loading of $Cu(DDC)_2$ into nanoparticles (NPs) only achieved low drug-loading efficiency and low drug concentration.[19] Recently, Metaplex technology or PRCosomes have been developed to prepare an injectable formulation of $Cu(DDC)_2$.[20] This breakthrough technology utilizes liposomes as a nanoscale reaction vessel to synthesize $Cu(DDC)_2$ NPs from copper ions ($Cu^{2+}$) and diethyldithiocarbamate ($DDC^-$) within the aqueous core of liposomes.[16] The in situ formed $Cu(DDC)_2$ NPs were incorporated inside liposomes and thus stabilized by liposome membranes. However, this method involves complicated preparation and purification processes, which will present difficulties and high expenses in large-scale manufacturing.

In this study, we developed a novel stabilized metal ion ligand complex (SMILE) technology to prepare $Cu(DDC)_2$ NPs. The SMILE technology involves a simple formulation and a straightforward, cost-effective preparation process, which thus can be easily scaled up during manufacturing and produce desirable $Cu(DDC)_2$ NPs at a reasonable price. This method could prepare $Cu(DDC)_2$ NPs with high drug concentrations, high loading efficiencies, and well-controlled physicochemical properties. We also investigated the anticancer activity and anticancer mechanism of the developed $Cu(DDC)_2$ NPs.

## 2. MATERIALS AND METHODS

**2.1. Materials.** 1,2-Distearoyl-*sn*-glycerol-3-phosphoethanolamine−poly(ethylene glycol) 2000 (DSPE−PEG) was purchased from NOF Corporation. Methoxy PEG 5000-*b*-poly(L-lactide) 5000 (PEG−PLA) was purchased from Polymer Source Inc. D-*α*-Tocopherol PEG 1000 succinate (TPGS) was purchased from Sigma-Aldrich. Other chemicals, solvents, and supplies were purchased from VWR International.

**2.2. Preparation of $Cu(DDC)_2$ NPs.** *2.2.1. Preparation of $Cu(DDC)_2$-Loaded Micelles.* $Cu(DDC)_2$-loaded micelles were prepared with a film-dispersion method as described in previous reports.[21−24] Briefly, 40 mg of micelle-forming materials and a given amount of $Cu(DDC)_2$ were dissolved in 0.5 mL of dichloromethane ($CH_2Cl_2$), and the solvent was removed under reduced pressure to form a film. The resulting film was hydrated in 1 mL deionized water and sonicated for 5 min. Unloaded $Cu(DDC)_2$ was removed by centrifugation at 12 000 rpm for 5 min. The supernatant was collected and filtered with 0.45 $\mu$M membrane filters.

*2.2.2. Preparation of $Cu(DDC)_2$ NPs with the SMILE Technology.* $Cu(DDC)_2$ NPs were prepared by mixing sodium diethyldithiocarbamatetrihydrate (DDC-Na) and copper chloride aqueous ($CuCl_2$) solution containing a stabilizer. The molar ratio between DDC-Na and $CuCl_2$ was 2:1. Briefly, DDC-Na and $CuCl_2$ were dissolved in 1% (w/v) stabilizer to get a DDC-Na solution and a $CuCl_2$ solution, respectively. Then, DDC-Na solution and $CuCl_2$ solution were mixed and vortexed for 1 min to form $Cu(DDC)_2$ NPs. The resulting NP formulation was centrifuged at 10 000 rpm for 10 min and filtered with the 0.45 $\mu$M membrane to remove large aggregations (Scheme 1).

**2.3. Determination of Particle Size and Morphology.** *2.3.1. Particle Size.* The particle size and size distribution of NPs


DOI: 10.1021/acsami.8b14940
ACS Appl. Mater. Interfaces XXXX, XXX, XXX−XXX

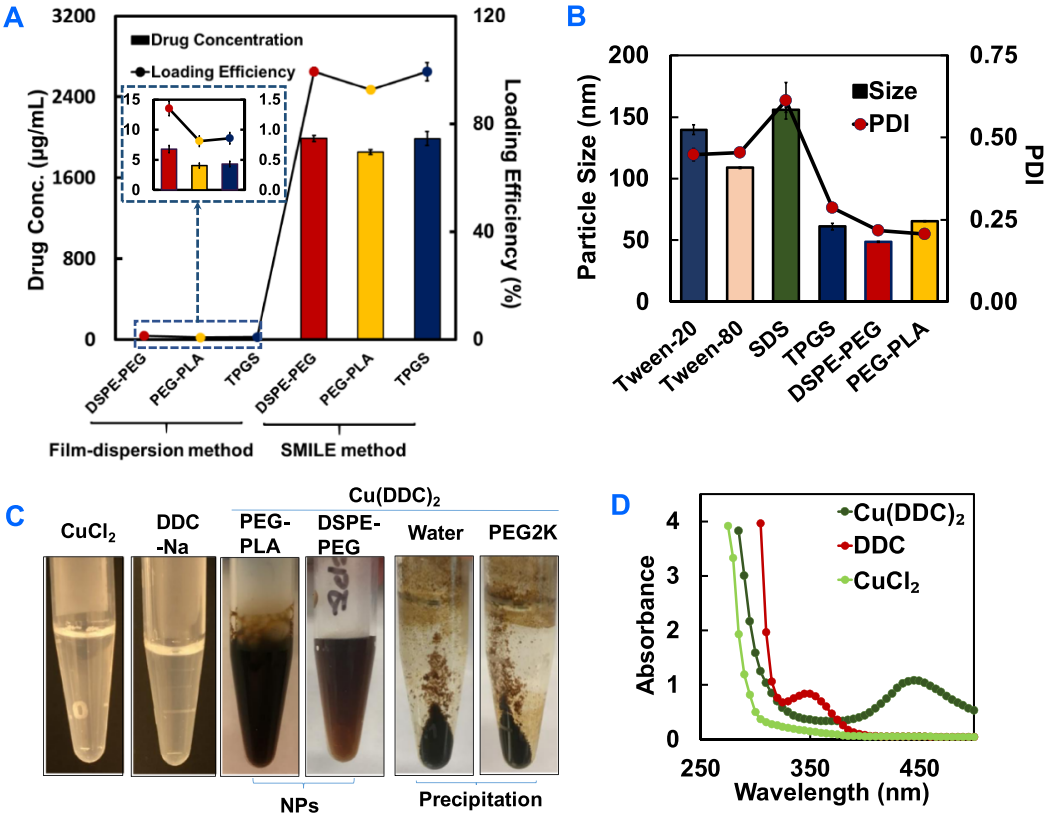


**Figure 1.** (A) Drug concentration and loading efficiency of $Cu(DDC)_2$ micelles prepared with a film-dispersion method (polymer 20 mg/mL) and $Cu(DDC)_2$ NPs prepared with a SMILE method (polymer 10 mg/mL). Results are the mean ± SD ($n$ = 3). (B) Particle size and PDI of $Cu(DDC)_2$ NPs (2 mg/mL) prepared with different stabilizers (10 mg/mL). Results are the mean ± SD ($n$ = 3). (C) Photos of $CuCl_2$, DDC-Na, and $Cu(DDC)_2$ NPs with different stabilizers (e.g., PEG−PLA and DSPE−PEG). Precipitations formed in water without a stabilizer or with a poor stabilizer (e.g., PEG2000). (D) UV−visible spectrum of Cu $(DDC)_2$, DDC-Na, and $CuCl_2$.

were determined by dynamic light scattering (DLS) using the Malvern Nano ZS.[25] Briefly, a $Cu(DDC)_2$ NP sample (200 μL) was added to a microcuvette. The particle size and size distribution were determined based on DLS at a 173° scattering angle.

*2.3.2. Transmission Electron Microscope.* The morphology of NPs was characterized using a high-resolution transmission electron microscope (JEM-2100F, JEOL). Samples were loaded onto a grid and stained with 1% uranyl acetate. The grid was visualized under the electron microscope.

**2.4. Nuclear Magnetic Resonance.** $^1H$ NMR spectra were recorded on a Varian 400 MHz spectrometer using deuterated chloroform ($CDCl_3$) or deuterated water ($D_2O$) as a solvent.

**2.5. Drug Concentration and Loading Efficiency.** The concentration of $Cu(DDC)_2$ NPs was determined with a UV−vis spectrometer. Briefly, $Cu(DDC)_2$ NP samples were diluted with dimethylformamide, and the absorbance at 435 nm was determined. The $Cu(DDC)_2$ concentration was calculated based on the standard curve generated with different concentrations of $Cu(DDC)_2$. The drug-loading efficiency was calculated using the following equation:

$$\text{Drug loading efficiency (\%)} = (\text{actual drug concentration}/\text{theoretical drug concentration}) \times 100\%$$

**2.6. Determination of the Stability of $Cu(DDC)_2$ NPs.** *2.6.1. Serum Stability.* $Cu(DDC)_2$ NPs were mixed and incubated with 10% fetal bovine serum (FBS) at room temperature. The particle size was determined with DLS at the different time points.

*2.6.2. Long-Term Storage Stability.* $Cu(DDC)_2$ NPs were kept at room temperature, and drug concentrations were determined on different days during storage.

**2.7. MTT Cytotoxicity Assay.** MCF-7 breast cancer cells (ATCC) were cultured in a medium composed of Roswell Park Memorial Institute (RPMI) 1640 with 10% FBS and 1% antibiotic−antimycotic. MDA-MB-231 cells (ATCC) were cultured in a 1:1 mixture of Dulbecco's modified Eagle's medium and Ham's F-12 medium, with 10% FBS and 1% antibiotic−antimycotic. DU145-TXR drug-resistant prostate cancer cells were obtained from Dr. Evan Keller at the University of Michigan and cultured in a RPMI 1640 medium supplemented with 10% FBS, 1% antibiotic−antimycotic, and 40 nM paclitaxel. Cells were cultured at 37 °C in a humidified atmosphere containing 5% $CO_2$.

Cells were seeded into a 96-well plate at a density of 5000 cells/well and incubated overnight. Then, a series of different concentrations of $Cu(DDC)_2$ NPs diluted in a cell culture medium were prepared and added to each well (100 μL/well). At different time points, cytotoxicity was determined with the 3-(4,5-dimethylthiazol-2-yl)-2,5-diphenyl tetrazolium bromide (MTT) assay. The absorbance was determined with a microplate spectrophotometer at a wavelength of 570 nm and a reference wavelength of 670 nm. Cytotoxicity was calculated using the following equation:

$$\text{Cell viability (\%)} = (A_{\text{test}}/A_{\text{control}}) \times 100\%$$

The half-maximal inhibitory concentration ($IC_{50}$) was calculated with SigmaPlot software based on a dose−response curve.[26,27]

**2.8. Colony-Forming Assay.** Cells were seeded in a 24-well plate at a density of 500 cells per well and incubated overnight. Then, cells were treated with different formulations for 2 h and further cultured in a fresh cell culture medium for 1 week. Colonies were fixed with 100% methanol and stained with crystal violet.[28]

**2.9. Determination of Intracellular Reactive Oxygen Species.** The generation of reactive oxygen species (ROS) was determined with a 2′,7′-dichlorodihydrofluorescein diacetate


DOI: 10.1021/acsami.8b14940
ACS Appl. Mater. Interfaces XXXX, XXX, XXX−XXX

(H2DCFDA) dye method.[29] Briefly, cells were seeded in a dark-walled, clear-bottomed 96-well plate with 50 000 cells per well and incubated at 37 °C overnight before study. Cells were incubated with 20 μM H2DCFDA in Hank's buffered salt solution (HBSS, pH = 7.4) for 30 min at 37 °C in the dark and treated with different formulations. Then, fluorescence was determined with a Cytation 5 Imaging Reader at $EX_{485nm}/EM_{535nm}$.

**2.10. Live/Dead Staining with Calcein-AM/Propidium Iodide.** Cells were seeded at a density of 5000 cells per well in a 96-well plate. After overnight incubation, cells were treated with different formulations for 24 h and then stained with a solution composed of calcein-AM and propidium iodide (PI) in pH 7.4 phosphate-buffered saline (PBS). Cell samples were analyzed with a Cytation 5 Cell Imaging Multi-Mode Reader. Viable and dead cells can be identified by the green fluorescence (viable) and the red fluorescence (dead), respectively. The fluorescence intensities were determined quantitatively at $EX_{480nm}/EM_{530nm}$ (viable cells) and $EX_{530nm}/EM_{620nm}$ (dead cells).

**2.11. Caspase 3/7 Activities.** Cells were seeded in a 96-well plate at a density of 20 000 cells per well and incubated overnight. After treating cells with different formulations, the culture medium was removed and 70 μL Caspase Glo 3 reagent (Promega, Madison, WI) was added to each well. After gently mixing the content in each well, the plate was incubated at room temperature for 30 min under dark conditions. Finally, 50 μL of the reaction solution was measured using a luminometer (Cytation 5 Imaging Reader).[27,30]

**2.12. Cell Morphology.** Cells seeded in a 96-well plate were treated with $Cu(DDC)_2$ NPs. The NP-induced change of cell morphology was observed with a Cytation 5 Cell Imaging Multi-Mode Reader. We also cotreated cells with cycloheximide (CHX, a protein synthesis and paraptosis inhibitor) or chloroquine (CQ, an autophagy inhibitor) and observed their effects on $Cu(DDC)_2$ NP-induced cell morphology change.

**2.13. Endoplasmic Reticulum Staining.** Cells were stained with endoplasmic reticulum (ER)-specific dye and Hoechst 33342 prior to microscopy. Briefly, cells were seeded in a clear-bottomed, black-walled 96-well plate at a density of 20 000 cells per well. After treatment with different formulations for 8 h, cells were incubated with a staining solution containing ER track dye (ER-ID green, Enzo Life Sciences Inc.) and Hoechst 33342 for 30 min at 37 °C avoiding light. Then, cells were washed with PBS and observed under a fluorescence microscope.

## 3. RESULTS

**3.1. Preparation of $Cu(DDC)_2$ NPs with the SMILE Method.** Because of the poor water solubility of $Cu(DDC)_2$, there is an emerging need to develop an injectable formulation for its clinical use.[16,17] In this study, we first attempted to use a classical film-dispersion method to prepare $Cu(DDC)_2$-loaded micelles. However, the drug-loading efficiency was extremely low. The drug concentrations varied among different polymers tested, but none of them achieved satisfactory drug concentration and loading efficiency. The resulted drug concentration was below 10 μg/mL, and the drug-loading efficiency was below 2% (left columns and the inserted panel in Figure 1A). Therefore, we developed the SMILE technology as an innovative method to prepare $Cu(DDC)_2$ NPs. With the SMILE method, we successfully prepared $Cu(DDC)_2$ NPs with a high drug concentration (2 mg/mL) and a high loading efficiency (close to 100%) using different stabilizers including DSPE−PEG, PEG−PLA, and TPGS (Figure 1A). We also extensively investigated the effects of theoretical drug concentrations and different stabilizers on actual drug concentrations and loading efficiencies (Figures S1 and S2). At the theoretical drug concentrations of 2 or 4 mg/mL, both TPGS and DSPE−PEG at concentrations ranging from 0.5 to 4% could all generate NPs with high drug-loading efficiency (close to 100%). The drug-loading efficiency was slightly lower in 4 mg/mL theoretical drug concentration groups compared to that in the 2 mg/mL groups. When the polymer stabilizer concentrations were at high levels (e.g., 2 or 4% of TPGS and DSPE−PEG, respectively), those groups with lower theoretical drug concentrations (e.g., 0.5 and 1 mg/mL of $Cu(DDC)_2$) showed significantly decreased $Cu(DDC)_2$ drug-loading efficiencies. However, when the polymer stabilizer concentrations were at low levels (e.g., 0.5 or 1%), those groups with similar low theoretical drug concentrations (e.g., 0.5 and 1 mg/mL of $Cu(DDC)_2$) showed much higher drug-loading efficiencies.

We also studied the effects of theoretical drug concentration and stabilizer concentration on the particle size and polydispersity index (PDI). When the theoretical drug concentration was 2 or 4 mg/mL, NPs exhibited a size of 60−70 nm if prepared with the TPGS stabilizer at the concentrations ranging from 0.5 to 4%. These NPs also showed a good size distribution as indicated by the small PDI value (Figure S3). However, when the theoretical drug concentration was set to be 1 or 0.5 mg/mL, the particle size varied significantly depending on the concentrations of TPGS used. These NPs also showed large PDI values, indicating a broad particle size distribution. A similar trend was also observed in NPs prepared with DSPE−PEG as the stabilizer. We could prepare NPs of well-controlled particle size when theoretical drug concentrations were 2 or 4 mg/mL with DSPE−PEG at concentrations ranging from 0.5 to 4%. The particle sizes were in the range of 40−80 nm depending on the DSPE−PEG and drug concentrations (Figure S4). All these NPs showed a narrow particle size distribution (small PDI value). At lower theoretical drug concentrations (0.5 or 1 mg/mL), NPs showed a large variation of particle sizes and large PDI values. These results suggested that the interaction between $DDC^-$ and $Cu^{2+}$ during the complex formation was critical for the NP preparation. This interaction is greatly influenced by the concentrations of $DDC^-$ and $Cu^{2+}$. Although stabilizers are essential for the preparation and stabilization of $Cu(DDC)_2$ NPs, high concentrations of stabilizers (e.g., 2 or 4%) may interfere with the interaction between $DDC^-$ and $Cu^{2+}$ and thus have a negative impact on the NP formation. These negative effects were more significant at lower concentrations of $DDC^-$ and $Cu^{2+}$. Therefore, the optimized theoretical drug concentration (2 mg/mL) and stabilizer concentration (1%) were used in the rest of the study unless otherwise specified.

We further explored the preparation of $Cu(DDC)_2$ NPs with additional stabilizers including Tween-20, Tween-80, and sodium dodecyl sulfate. All of these stabilizers could be successfully used to prepare $Cu(DDC)_2$ NPs with particle sizes ranging from 50 to 150 nm. The selection of stabilizers had a pronounced impact on the particle size and PDI (Figure 1B). Compared with the micelle solutions of DSPE and TPGS, the corresponding $Cu(DDC)_2$ NPs showed significant larger particle sizes. In contrast, the PEG−PLA micelle and PEG−PLA/$Cu(DDC)_2$ NPs had similar particle sizes (Figure S5). We characterized the blank PEG−PLA and PEG−PLA/$Cu(DDC)_2$ NPs using transmission electron microscopy (TEM). Both of them showed spherical morphology and similar particle sizes (Figure S6).

The formation of $Cu(DDC)_2$ NPs was also confirmed by colorimetric visualization and by UV−vis spectroscopy. The SMILE method produced stable $Cu(DDC)_2$ NPs with a dark


DOI: 10.1021/acsami.8b14940
ACS Appl. Mater. Interfaces XXXX, XXX, XXX−XXX

color in the presence of appropriate stabilizers (e.g., PEG−PLA and DSPE−PEG), while precipitation formed with a poor stabilizer or without a stabilizer (Figure 1C). The UV−vis spectrum showed that $Cu(DDC)_2$ has a characteristic peak of around 450 nm, which is absent in pure DDC-Na or $CuCl_2$ solutions (Figure 1D). We also used $^1H$ NMR spectroscopy to confirm the formation of NPs and study the structure of PEG−PLA $Cu(DDC)_2$ NPs (Figure 2). When all components were

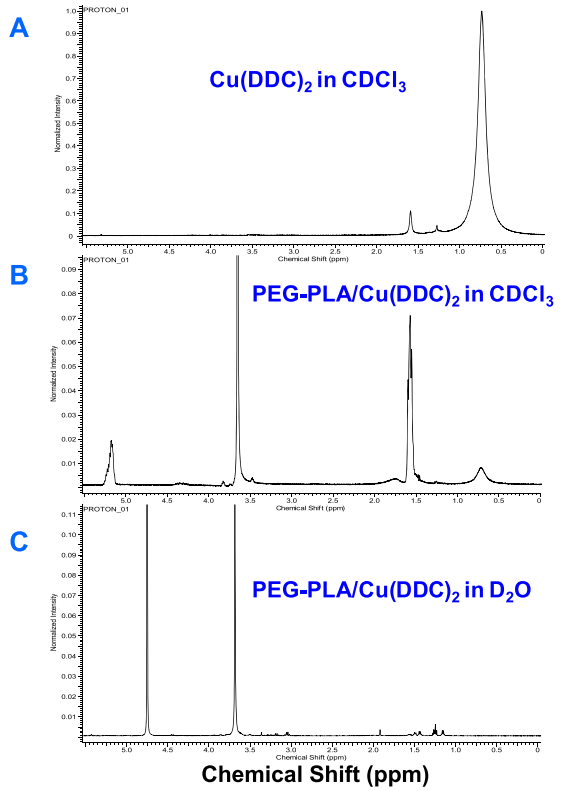


**Figure 2.** Core−shell structure of PEG−PLA $Cu(DDC)_2$ NPs. (A) $^1H$ NMR of $Cu(DDC)_2$ in $CDCl_3$; (B) $^1H$ NMR of PEG−PLA and $Cu(DDC)_2$ dissolved in $CDCl_3$; and (C) $^1H$ NMR of PEG−PLA/$Cu(DDC)_2$ NPs formed in $D_2O$. PEG−PLA and $Cu(DDC)_2$ concentrations in (B,C) were 10 and 2 mg/mL, respectively.

dissolved in $CDCl_3$, the peaks from the hydrophilic PEG block (3.6 ppm), the hydrophobic PLA block (5.1 and 1.7 ppm), and $Cu(DDC)_2$ (0.7 ppm) were all observed. When PEG−PLA $Cu(DDC)_2$ NPs were prepared in $D_2O$, the peaks corresponding to the hydrophobic PLA block and $Cu(DDC)_2$ were significantly diminished in contrast to the strong peaks for the hydrophilic PEG block. These results demonstrated that the PEG−PLA/$Cu(DDC)_2$ NPs had a core−shell structure with $Cu(DDC)_2$ embedded inside the hydrophobic core of PEG−PLA micelles. The PEG−PLA surrounding $Cu(DDC)_2$ NPs could stabilize the NPs and prevent aggregation formation.

The selection of stabilizers also had a great influence on NP stability. We determined the stability of NPs in the presence of 10% serum. PEG−PLA/$Cu(DDC)_2$ NPs showed excellent stability and did not have a significant change in particle size and PDI after incubation for at least 72 h. Although there was no obvious precipitation in TPGS and DSPE−PEG Cu-$(DDC)_2$ NP groups, particle sizes significantly increased over time (Figure 3A,B). We also determined the long-term stability of $Cu(DDC)_2$ NPs prepared with different stabilizers, including TPGS, DSPE−PEG, and PEG−PLA. NPs were kept at room temperature, and changes in drug concentration were determined. As shown in Figure 3C, PEG−PLA/$Cu(DDC)_2$ NPs demonstrated excellent stability with a minor decrease of drug concentration after 30 days of storage at room temperature. In contrast, the drug concentrations of DSPE−PEG and TPGS NPs were significantly decreased, indicating their poor storage stability.

**3.2. Anticancer Activity of $Cu(DDC)_2$ NPs.** The anticancer activity of $Cu(DDC)_2$ NPs in drug-resistant DU145-TXR cells was first determined using the MTT assay. As shown in Figure 4A, the DU145-TXR cell is resistant to paclitaxel with an $IC_{50}$ of 2575 nM. $Cu(DDC)_2$ NPs prepared with PEG−PLA, TPGS, and DSPE−PEG all showed potent anticancer activities at 48 h treatment. The $IC_{50}$ values were 85, 172, and 193 nM, respectively. The treatment of equivalent concentrations of $CuCl_2$, DDC-Na, blank PEG−PLA, blank DSPE−PEG, or TPGS did not show significant cell toxicity. The anticancer effects also depended on the treatment time with increased anticancer effects occurring after prolonged treatment. Cells treated with DSPE−PEG/$Cu(DDC)_2$ NPs showed an $IC_{50}$ of 216 nM at 24 h and 138 nM at 72 h (Figure 4B). Similarly, the cells treated with TPGS/$Cu(DDC)_2$ NPs showed an $IC_{50}$ of 280 nM at 24 h and 149 nM at 72 h (Figure 4C). $Cu(DDC)_2$ NPs also demonstrated excellent anticancer activity in other cancer cells including MDA-MB-231 cells and MCF-7 cells. The $IC_{50}$ values of TPGS/$Cu(DDC)_2$ NP and PEG−PLA $Cu(DDC)_2$ NPs on MDA-MB-231 cells were 123 and 104 nM, respectively (Figure 4D). We further tested cell viability based on calcein AM and PI staining of cancer cells treated with $Cu(DDC)_2$ NPs. The treatment caused a dose-dependent increase in membrane permeability. The red staining of dead cells increased with increasing drug concentrations. Concurrently, the green fluorescence signal of living cells decreased with increasing drug concentrations. These were evaluated qualitatively with fluorescence imaging (Figures 5A and S7) and quantitatively by determining green and red fluorescence intensities, respectively (Figure 5B). In addition, we probed the anticancer effects of $Cu(DDC)_2$ NPs with the colony formation assay. The treatment of blank PEG−PLA did not show any noticeable effects on colony formation by DU145-TXR cells. The treatment of PEG−PLA/$Cu(DDC)_2$ NPs showed significant inhibition of colony formation. The inhibition effects were significantly enhanced with the increased NP concentration. The colony formation was almost completely inhibited at the $Cu(DDC)_2$ NP concentration of 0.2 $\mu$M (Figure 5C).

**3.3. $Cu(DDC)_2$ NP-Induced Cell Death through Paraptosis.** The anticancer mechanisms of DSF and the DSF/copper combination have been investigated in multiple studies.[31−33] The proteasome/poly-Ub protein degradation pathway has been recognized as one of the major targets.[9,10] The morphology of DU145-TXR cells was observed under a bright-field microscope. The $Cu(DDC)_2$ NPs included extensive cytoplasmic vacuolation in DU145-TXR cells (Figure S8). The vacuoles could be observed as early as 8 h after the treatment and continuously increased in size. Cytoplasmic vacuolation was also observed in $Cu(DDC)_2$ NP-treated MCF-7 cells (Figure S9). To examine the origin of the vacuoles, cells were stained with ER-tracker dyes. As shown in Figure 6A, ER in the control cells or those treated with paclitaxel (0.5 $\mu$M) had a typical reticulate structure. The treatment of $Cu(DDC)_2$ NPs induced the formation of cytoplasmic vacuoles, which were positive for ER-specific markers, indicating that they


DOI: 10.1021/acsami.8b14940
ACS Appl. Mater. Interfaces XXXX, XXX, XXX−XXX

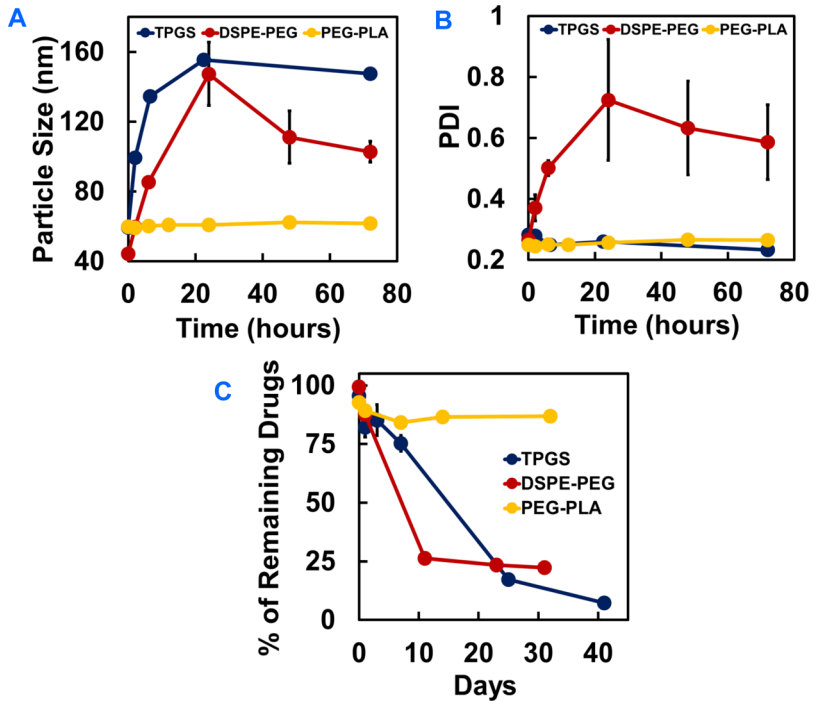


**Figure 3.** $Cu(DDC)_2$ NP stability. NPs prepared with different stabilizers were incubated in 10% FBS in PBS solution. Particle size (A) and PDI (B) were determined at different time points. (C) Storage stability of $Cu(DDC)_2$ NPs. NPs were kept at room temperature, and $Cu(DDC)_2$ concentration was determined at different time points. Results are the mean ± SD ($n$ = 3).

originated from the ER. The treatment of an autophagy inhibitor, CQ, did not show any significant effects on $Cu(DDC)_2$ NP-induced cytoplasmic vacuolation, proving that cytoplasmic vacuolization was not caused by autophagosome accumulation (Figure 6B). In contrast, cytoplasmic vacuolation was inhibited by the cotreatment with CHX, an inhibitor of paraptosis (Figure 6B). The inhibition of cytoplasmic vacuolization was also observed after 24 h of treatment (Figure S10).

The paraptosis is caspase-independent cell death. Therefore, we also determined caspase 3/7 activities of DU145-RXR cells treated with $Cu(DDC)_2$ NPs. The treatment with $Cu(DDC)_2$ NPs (0.5 $\mu$M) did not cause significant increase of caspase 3/7 activities compared to a negative control group of cells treated with an equivalent amount of PEG−PLA. However, the doxorubicin (20 $\mu$M) and lapatinib (10 $\mu$M) combination-treated cells showed a significant higher caspase 3/7 activity (Figure 7A). In addition, we examined the induction of intracellular ROS in DU145-TXR cells. As shown in Figure 7B, the treatment of $Cu(DDC)_2$ NPs (5.5 or 0.55 $\mu$M) did not increase the ROS levels compared with the negative control HBSS-treated group, though the ROS level was increased in the $H_2O_2$ (100 $\mu$M) positive control-treated group.

## 4. DISCUSSION

In this study, we developed an innovative SMILE technology to prepare $Cu(DDC)_2$ NP formulations with high drug concentration and high drug-loading efficiency. The drug concentration achieved with this method is at least 2 mg/mL, which will meet the needs for in vivo applications. $Cu(DDC)_2$ NPs were formed in situ by mixing DDC-Na and $CuCl_2$ in the presence of a stabilizer. Stabilizers successfully used in this method for NP preparation include excipients from the FDA-approved generally recognized as safe excipient list or those with well-accepted safety profiles. The use of these excipients can avoid potential safety and other regulatory concerns associated with excipients. In addition, the SMILE technology is also a "green" method for NP preparation without using toxic organic solvents. The fabrication of $Cu(DDC)_2$ NPs with the SMILE technology does not involve complicated NP preparation nor postpreparation purification process. The complicated production process is a notorious obstacle for the commercialization of nanotechnology drug products. The SMILE technology provided an innovative solution to solve this problem and pave the way for its clinical translation and commercialization. We could further improve the fabrication process using microfluidics-based mixers, which should have an even better control of the mixing process and improve the properties of NPs. The SMILE technology can also be easily scaled up for mass production. All of the above advantages of SMILE technology would make it a promising method for preparing $Cu(DDC)_2$ NPs with great potential for clinical use.

The selection of stabilizers has a great influence on the physical−chemical properties of $Cu(DDC)_2$ NPs including particle size, drug-loading efficiency, and stability. The amphiphilic nature of stabilizers (i.e., surfactant-like materials) is critical for the formation and stabilization of $Cu(DDC)_2$ NPs. The use of hydrophilic polymers (such as PEG) resulted in the lack of $Cu(DDC)_2$ NP formation. The presence of amphiphilic stabilizers could prevent the uncontrolled growth of NPs and avoid the formation of large aggregations. The hydrophobic moieties of the stabilizers interact with $Cu(DDC)_2$ NPs, and the hydrophilic block forms a steric protection layer on the surface of NPs. As a result, a core−shell-structured nanoassembly was formed. This core−shell structure of NPs was confirmed by the $^1$H NMR in our study (Figure 2). The interaction between a hydrophobic component of stabilizers and $Cu(DDC)_2$ NPs is an important factor


DOI: 10.1021/acsami.8b14940
ACS Appl. Mater. Interfaces XXXX, XXX, XXX−XXX

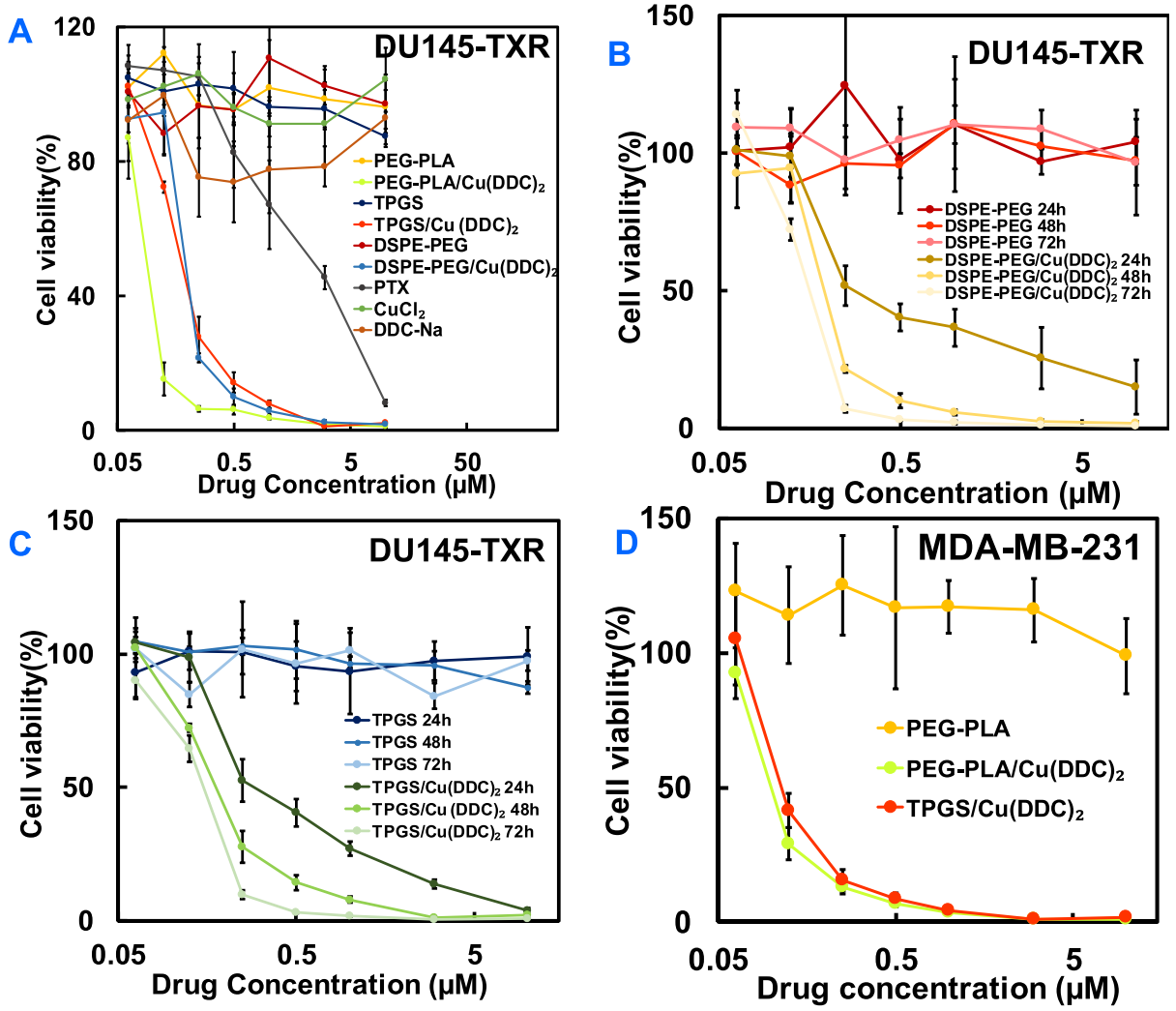


**Figure 4.** MTT assay. (A) DU145-TXR cells were treated with different formulations for 48 h. DU145-TXR treated with DSPE−PEG/$Cu(DDC)_2$ NPs (B) and TPGS/$Cu(DDC)_2$ (C) for 24, 48, and 72 h. (D) MDA-MB-231 cells treated with $Cu(DDC)_2$ NPs for 48 h. Results are the mean ± SD ($n$ = 4).

for the NP preparation. In our study, the use of PEG 2000 ($PEG_{2K}$) failed to form $Cu(DDC)_2$ NPs, although PEG has been used in multiple studies to improve the NP stabilities and prevent their aggregation. This is probably due to the lack of hydrophobic components in the PEG, which was unable to have strong hydrophobic interactions with $Cu(DDC)_2$ NPs. The difference in the interactions between stabilizers and $Cu(DDC)_2$ could also explain the varied stabilities of NPs prepared with different stabilizers such as PEG−PLA, TPGS, and DSPE−PEG. Stabilizers with a large hydrophobic component (e.g., PEG−PLA) could result in stronger interactions with $Cu(DDC)_2$ than TPGS or DSPE−PEG, which have relatively smaller hydrophobic components. Therefore, we could engineer the hydrophobic components of stabilizers to improve their performances in preparing $Cu(DDC)_2$ NPs.

The PEG−PLA $Cu(DDC)_2$ NPs developed in this study demonstrated excellent storage stability and serum stability. We could further improve the stability by designing and screening additional stabilizers, which might show stronger interactions with $Cu(DDC)_2$. A freeze-dried formulation could also be an option for its clinical application. Another alternative is that $Cu(DDC)_2$ NPs could be prepared immediately before use. Because of the simple and straightforward preparation method, a kit could be developed to allow the preparation of $Cu(DDC)_2$ NPs by health-care practitioners without extensive special training.

In this study, $Cu(DDC)_2$ NPs demonstrated excellent anticancer activity against drug-resistant prostate DU145-TXR cells. The drug resistance is a significant issue for prostate cancer treatment. The development of $Cu(DDC)_2$ NPs will potentially lead to a novel effective and affordable drug for patients with drug-resistant prostate cancers. $Cu(DDC)_2$ NPs also showed activity against MCF-7 breast cancer as well as triple negative MDA-MB-231 breast cancer cells, indicating its potential as a broad spectrum anticancer agent. The anticancer mechanism of DSF or DSF/Cu combination has been investigated in several previous studies. DSF/Cu can inhibit proteasome/poly-Ub protein degradation pathway by targeting the NPL4 protein, which is upstream to the proteasome.[9,10] Briefly, $Cu(DDC)_2$ binds to the NPL4 protein, induces NPL4-P97 aggregation, and disables the P97-NPL4-UFD1 pathway. The inhibition of poly-Ub protein degradation leads to poly-Ub protein accumulation in the ER, thereby causing ER stress and unfolded protein response,[9] increases intracellular $Ca^{2+}$ concentration,[34] impairs mitochondria


DOI: 10.1021/acsami.8b14940
ACS Appl. Mater. Interfaces XXXX, XXX, XXX−XXX

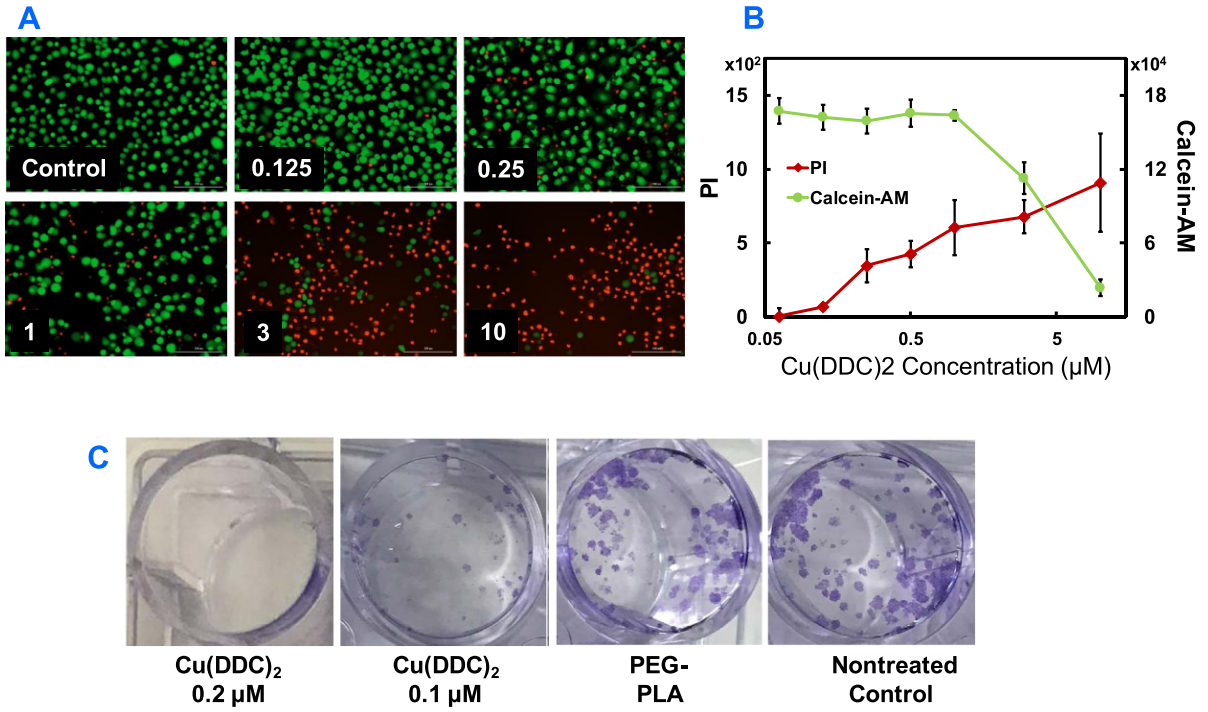


**Figure 5.** Calcein-AM/PI staining. DU145-TXR cells in a 96-well plate were treated with various concentrations ($\mu$M) of TPGS/$Cu(DDC)_2$ NPs as well as a negative control (TPGS only). Twenty-four hours after treatment, cells were stained with calcein-AM and PI and then analyzed by using fluorescence imaging (A) and by determining fluorescence intensity (B). Results are the mean ± SD ($n$ = 4). (C) Cell colony assay. DU145-TXR cells were seeded at a density of 500 cells per well. The following day, cells were treated with 0.2 or 0.1 $\mu$M PEG−PLA/$Cu(DDC)_2$ and blank PEG−PLA for 2 h. Cells were cultured for 1 additional week. Cell colonies were fixed with methanol and visualized with crystal violet staining.

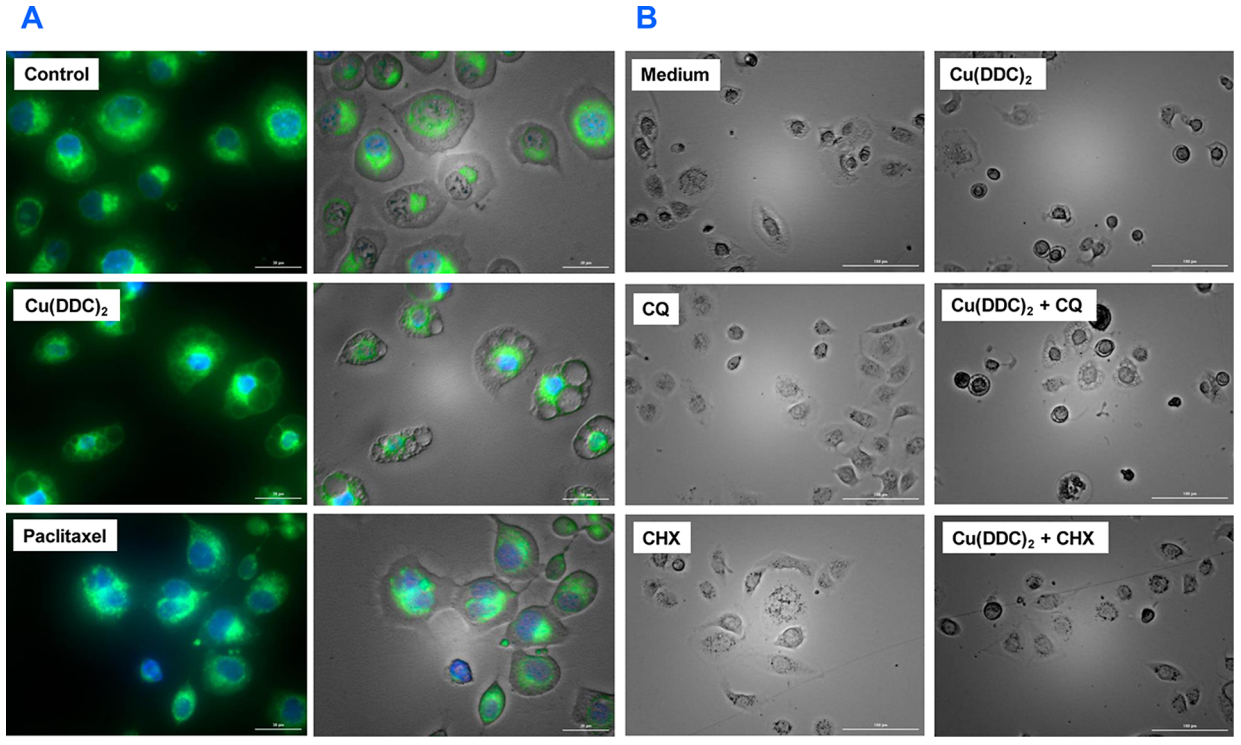


**Figure 6.** $Cu(DDC)_2$ NPs induced cell paraptosis. (A) DU145-TXR cells were treated with blank PEG−PLA, paclitaxel (0.5 $\mu$M), or PEG−PLA/$Cu(DDC)_2$ NPs (0.5 $\mu$M) for 8 h and stained with ER-ID green dye and Hoechst 33342. PEG−PLA/$Cu(DDC)_2$ NPs treatment induced cytoplasmic vacuolation resulted from dilated ER. Right panel: Merged fluorescence and bright filed images. (B) Morphology of Du145-TXR cells treated with $Cu(DDC)_2$ NPs (0.5 $\mu$M) alone and in combination with CHX (20 $\mu$M) or CQ (20 $\mu$M) for 8 h.

function,[35] and finally causes cell death via apoptosis or nonapoptotic cell death (e.g., paraptosis and autophagy).[36]

Apoptosis is a type of cell death demonstrating hallmarks such as caspase activation, chromatin condensation, nuclear


DOI: 10.1021/acsami.8b14940
ACS Appl. Mater. Interfaces XXXX, XXX, XXX−XXX

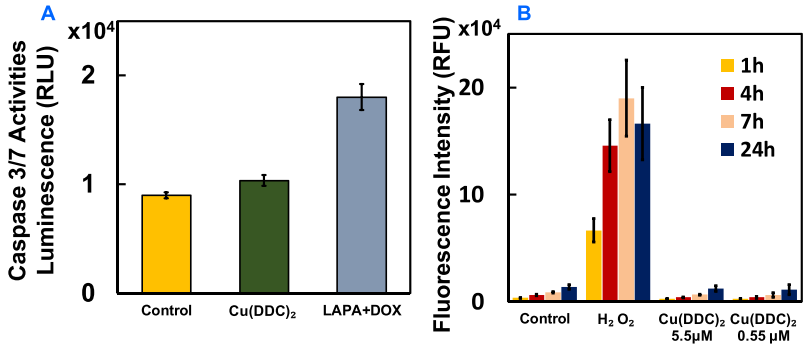


**Figure 7.** (A) Effects of $Cu(DDC)_2$ NP treatment on caspase 3/7 activation. Cells were treated with blank PEG−PLA, $Cu(DDC)_2$ NPs (0.5 $\mu$M), and lapatinib (10 $\mu$M) + doxorubicin (20 $\mu$M) for 24 h. Caspase 3/7 activities were determined with Caspase-Glo 3/7 assay. Results are the mean ± SD ($n$ = 4). (B) Effects of $Cu(DDC)_2$ NP treatment on ROS generation. DU145-TXR cells were treated with 5.5 $\mu$M $Cu(DDC)_2$ NPs, 0.55 $\mu$M $Cu(DDC)_2$ NPs, 100 $\mu$M $H_2O_2$ (positive control), and PBS (negative control). ROS was determined with 2′,7′-dichlorofluorescein diacetate method after treating cells with different formulations for different lengths of time. Results are the mean ± SD ($n$ = 4).

fragmentation, and formation of apoptotic bodies. Some studies reported that apoptosis was involved in the DSF/Cu-induced cell death.[35] However, others showed that DSF or $Cu(DDC)_2$ may inhibit caspase activation and block cell apoptosis.[37,38] A recent study also showed that DSF/Cu induced cell apoptosis in a cell-type-specific manner.[9] In the current study, we found that treatment with $Cu(DDC)_2$ did not significantly increase the caspase 3/7 activity, indicating that caspase-mediated apoptosis might not be a major cell death pathway for DU145-TXR cells treated with $Cu(DDC)_2$ NPs. Instead, the treatment of $Cu(DDC)_2$ NPs induced cytoplasmic vacuolation, which is a typical morphology of paraptosis. The vacuole formation was effectively inhibited by cotreatment with a paraptosis inhibitor but not an autophagy inhibitor. This further confirmed that paraptosis rather than autophagy was the major pathway involved in the $Cu(DDC)_2$ NP-induced cell death in DU145-TXR cells. This result is consistent with several previous reports, which showed that copper complexes induced paraptosis, a type of nonapoptotic programmed cell death.[38−41] Paraptosis is featured with cell cytoplasm vacuoles derived from swelled ER. Our studies with ER-specific staining also indicated the ER origin of the cytoplasm vacuoles. During the paraptosis process, cytoplasm vacuoles increase in number and size. Large vacuoles surrounding the intact nuclei form at the late stage. Eventually, cells rupture and release substances, which may cause inflammation or stimulate anticancer immune responses. Unlike apoptosis, paraptosis does not show chromatin condensation, nuclear fragmentation, or caspase activities. Paraptosis is a promising target for cancer therapy, particularly, for resistant cancers with defective cell apoptosis pathways. To further characterize cell paraptosis, we could trace the paraptosis vacuoles on cells overexpressing fluorescent protein-tagged ER or use immunocytochemistry approach to label ER with an antibody against protein disulfide isomerase (PDI). Although we observed the formation of paraptosis vacuoles in DU145-TXR cells and MCF-7 breast cancer cells as well, this might be cell-type-specific. Therefore, further studies will still be needed to further verify this in additional prostate cancer cells as well as other cancer cells before we could draw a more general conclusion.

## 5. CONCLUSIONS

In conclusion, we have developed a SMILE technology as an innovative method to prepare $Cu(DDC)_2$ NPs. These NPs demonstrated great potential as an anticancer agent to treat drug-resistant prostate cancer as well as other types of cancers. $Cu(DDC)_2$ NP treatment effectively induced cancer cell death through paraptosis. The NP formulation developed in the current study has a great potential as a new generation of nanotherapeutics for treating drug-resistant prostate cancer and benefit prostate cancer patients. In the future, the optimized formulation will be further evaluated with additional preclinical animal studies to determine in vivo pharmacokinetics, anticancer efficacy, and safety profile.

## ■ ASSOCIATED CONTENT

### Supporting Information

The Supporting Information is available free of charge on the ACS Publications website at DOI: 10.1021/acsami.8b14940.

Effects of theoretical drug concentration and TPGS concentration on actual $Cu(DDC)_2$ drug concentration and drug-loading efficiency; effects of theoretical drug concentration and DSPE−PEG concentration on actual $Cu(DDC)_2$ drug concentration and drug-loading efficiency; effects of theoretical drug concentration and TPGS concentration on NP particle size and PDI; effects of theoretical drug concentration and DSPE−PEG concentration on NP particle size and PDI; particle size of 2 mg/mL $Cu(DDC)_2$ NPs and corresponding stabilizers without $Cu(DDC)_2$ NPs; TEM of PEG−PLA micelles and PEG−PLA/$Cu(DDC)_2$ NPs; calcein AM/PI staining of DU145-TXR cells treated with $Cu(DDC)_2$ NPs; morphology of DU145-TXR cells treated with $Cu(DDC)_2$ NPs (0.5 $\mu$M), paclitaxel (0.5 $\mu$M), and blank PEG−PLA for 24 h; morphology of MCF-7 cells treated with 0.5 $\mu$M DSPE−PEG/$Cu(DDC)_2$ NPs for 72 h; and morphology of Du145-TXR cells treated with $Cu(DDC)_2$ NPs (0.5 $\mu$M) alone and in combination with CHX (20 $\mu$M) or CQ (20 $\mu$M) for 24 h (PDF)

## ■ AUTHOR INFORMATION

### Corresponding Authors

*E-mail: yzhuang@simm.ac.cn. Phone: +86-21-2023-1981 (Y.H.).

*E-mail: FZL0023@auburn.edu. Phone: 334-844-7406 (F.L.).

### ORCID

Pengyu Chen: 0000-0003-3380-872X

Yongzhuo Huang: 0000-0001-7067-8915



DOI: 10.1021/acsami.8b14940
ACS Appl. Mater. Interfaces XXXX, XXX, XXX−XXX

Feng Li: 0000-0002-8559-3831

### Notes

The authors declare no competing financial interest.

## ■ ACKNOWLEDGMENTS

This work was financially supported by Auburn University startup fund (F.L.) and National Science Foundation grant no. CBET-1701363 (P.C.). A sincere thank you to Dr. Deadre Johnson for proofreading of this paper.

## ■ REFERENCES

(1) Basch, E.; Loblaw, D. A.; Rumble, R. B. Systemic Therapy in Men With Metastatic Castration-Resistant Prostate Cancer: American Society of Clinical Oncology and Cancer Care Ontario Clinical Practice Guideline Summary. *J. Oncol. Pract.* **2014**, *10*, e418−e420.

(2) Hwang, C. Overcoming Docetaxel Resistance in Prostate Cancer: a Perspective Review. *Ther. Adv. Med. Oncol.* **2012**, *4*, 329−340.

(3) Theyer, G.; Schirmböck, M.; Thalhammer, T.; Sherwood, E. R.; Baumgartner, G.; Hamilton, G. Role of the MDR-1-encoded Multiple Drug Resistance Phenotype in Prostate Cancer Cell Lines. *J. Urol.* **1993**, *150*, 1544−1547.

(4) van Brussel, J. P.; Mickisch, G. H. J. Multidrug Resistance in Prostate Cancer. *Oncol. Res. Treat.* **2003**, *26*, 175−181.

(5) Li, F.; Mahato, R. I. MicroRNAs and Drug Resistance in Prostate Cancers. *Mol. Pharm.* **2014**, *11*, 2539−2552.

(6) Li, F.; Mahato, R. I. miRNAs as Targets for Cancer Treatment: Therapeutics Design and Delivery. Preface. *Adv. Drug Deliv. Rev.* **2015**, *81*, 5−6.

(7) Sleire, L.; Førde, H. E.; Netland, I. A.; Leiss, L.; Skeie, B. S.; Enger, P. Ø. Drug Repurposing in Cancer. *Pharmacol. Res.* **2017**, *124*, 74−91.

(8) Lun, X.; Wells, J. C.; Grinshtein, N.; King, J. C.; Hao, X.; Dang, N.-H.; Wang, X.; Aman, A.; Uehling, D.; Datti, A.; Wrana, J. L.; Easaw, J. C.; Luchman, A.; Weiss, S.; Cairncross, J. G.; Kaplan, D. R.; Robbins, S. M.; Senger, D. L. Disulfiram when Combined with Copper Enhances the Therapeutic Effects of Temozolomide for the Treatment of Glioblastoma. *Clin. Cancer Res.* **2016**, *22*, 3860−3875.

(9) Skrott, Z.; Mistrik, M.; Andersen, K. K.; Friis, S.; Majera, D.; Gursky, J.; Ozdian, T.; Bartkova, J.; Turi, Z.; Moudry, P.; Kraus, M.; Michalova, M.; Vaclavkova, J.; Dzubak, P.; Vrobel, I.; Pouckova, P.; Sedlacek, J.; Miklovicova, A.; Kutt, A.; Li, J.; Mattova, J.; Driessen, C.; Dou, Q. P.; Olsen, J.; Hajduch, M.; Cvek, B.; Deshaies, R. J.; Bartek, J. Alcohol-abuse Drug Disulfiram Targets Cancer via p97 Segregase Adaptor NPL4. *Nature* **2017**, *552*, 194−199.

(10) Brüning, A.; Kast, R. E. Oxidizing to death. *Cell Cycle* **2014**, *13*, 1513−1514.

(11) Wang, Z.; Tan, J.; McConville, C.; Kannappan, V.; Tawari, P. E.; Brown, J.; Ding, J.; Armesilla, A. L.; Irache, J. M.; Mei, Q.-B.; Tan, Y.; Liu, Y.; Jiang, W.; Bian, X.-W.; Wang, W. Poly Lactic-co-glycolic Acid Controlled Delivery of Disulfiram to Target Liver Cancer Stem-like Cells. *Nanomedicine* **2017**, *13*, 641−657.

(12) Liu, P.; Kumar, I. S.; Brown, S.; Kannappan, V.; Tawari, P. E.; Tang, J. Z.; Jiang, W.; Armesilla, A. L.; Darling, J. L.; Wang, W. Disulfiram Targets Cancer Stem-like Cells and Reverses Resistance and Cross-resistance in Acquired Paclitaxel-resistant Triple-negative Breast Cancer Cells. *Br. J. Cancer* **2013**, *109*, 1876−1885.

(13) Loo, T. W.; Clarke, D. M. Blockage of Drug Resistance in vitro by Disulfiram, a Drug Used to Treat Alcoholism. *J. Natl. Cancer Inst.* **2000**, *92*, 898−902.

(14) https://clinicaltrials.gov (NCT02963051, NCT02678975, NCT03363659).

(15) Pushpakom, S.; Iorio, F.; Eyers, P. A.; Escott, K. J.; Hopper, S.; Wells, A.; Doig, A.; Guilliams, T.; Latimer, J.; McNamee, C.; Norris, A.; Sanseau, P.; Cavalla, D.; Pirmohamed, M. Drug Repurposing: Progress, Challenges and Recommendations. *Nat. Rev. Drug Discov.* **2018**, DOI: 10.1038/nrd.2018.168.

(16) Wehbe, M.; Anantha, M.; Shi, M.; Leung, A. W.-y.; Dragowska, W.; Sanche, L.; Bally, M. Development and Optimization of an Injectable Formulation of Copper Diethyldithiocarbamate, an Active Anticancer Agent. *Int. J. Nanomed.* **2017**, *12*, 4129−4146.

(17) Zhao, P.; Yin, W.; Wu, A.; Tang, Y.; Wang, J.; Pan, Z.; Lin, T.; Zhang, M.; Chen, B.; Duan, Y.; Huang, Y. Dual-Targeting to Cancer Cells and M2 Macrophages via Biomimetic Delivery of Mannosylated Albumin Nanoparticles for Drug-Resistant Cancer Therapy. *Adv. Funct. Mater.* **2017**, *27*, 1700403.

(18) Marengo, A.; Forciniti, S.; Dando, I.; Dalla Pozza, E.; Stella, B.; Tsapis, N.; Yagoubi, N.; Fanelli, G.; Fattal, E.; Heeschen, C.; Palmieri, M.; Arpicco, S. Pancreatic Cancer Stem Cell Proliferation is Strongly Inhibited by Diethyldithiocarbamate-copper Complex Loaded into Hyaluronic Acid Decorated Liposomes. *Biochim. Biophys. Acta, Gen. Subj.* **2018**, *1863*, 61−72.

(19) Zhao, P.; Wang, Y.; Kang, X.; Wu, A.; Yin, W.; Tang, Y.; Wang, J.; Zhang, M.; Duan, Y.; Huang, Y. Dual-targeting Biomimetic Delivery for Anti-glioma Activity via Remodeling the Tumor Microenvironment and Directing Macrophage-mediated Immunotherapy. *Chem. Sci.* **2018**, *9*, 2674−2689.

(20) Wehbe, M.; Chernov, L.; Chen, K.; Bally, M. B. PRCosomes: Pretty Reactive Complexes Formed in Liposomes. *J. Drug Target.* **2016**, *24*, 787−796.

(21) Wang, H.; Li, F.; Du, C.; Wang, H.; Mahato, R. I.; Huang, Y. Doxorubicin and Lapatinib Combination Nanomedicine for Treating Resistant Breast Cancer. *Mol. Pharm.* **2014**, *11*, 2600−2611.

(22) Li, F.; Snow-Davis, C.; Du, C.; Bondarev, M. L.; Saulsbury, M. D.; Heyliger, S. O. Preparation and Characterization of Lipophilic Doxorubicin Pro-drug Micelles. *J. Visualized Exp.* **2016**, *114*, e54338.

(23) Li, F.; Danquah, M.; Singh, S.; Wu, H.; Mahato, R. I. Paclitaxel- and Lapatinib-loaded Lipopolymer Micelles Overcome Multidrug Resistance in Prostate Cancer. *Drug Delivery Transl. Res.* **2011**, *1*, 420−428.

(24) Lu, W.; Li, F.; Mahato, R. I. Poly(ethylene glycol)-block-poly(2-methyl-2-benzoxycarbonyl-propylene carbonate) Micelles for Rapamycin Delivery: in vitro Characterization and Biodistribution. *J. Pharm. Sci.* **2011**, *100*, 2418−2429.

(25) Li, F.; Danquah, M.; Mahato, R. I. Synthesis and Characterization of Amphiphilic Lipopolymers for Micellar Drug Delivery. *Biomacromolecules* **2010**, *11*, 2610−2620.

(26) Wang, C.-Y.; Li, F.; Yang, Y.; Guo, H.-Y.; Wu, C.-X.; Wang, S. Recombinant Baculovirus Containing theDiphtheria Toxin AGene for Malignant Glioma Therapy. *Cancer Res.* **2006**, *66*, 5798−5806.

(27) Li, F.; Lu, Y.; Li, W.; Miller, D. D.; Mahato, R. I. Synthesis, Formulation and in vitro Evaluation of a Novel Microtubule Destabilizer, SMART-100. *J. Controlled Release* **2010**, *143*, 151−158.

(28) Crowley, L. C.; Christensen, M. E.; Waterhouse, N. J. Measuring Survival of Adherent Cells with the Colony-Forming Assay. *Cold Spring Harb. Protoc.* **2016**, *2016*, pdb.prot087171.

(29) Wadhwa, S.; Mumper, R. J. Intracellular Delivery of the Reactive Oxygen Species Generating Agentd-Penicillamine upon Conjugation to Poly-l-glutamic Acid. *Mol. Pharm.* **2010**, *7*, 854−862.

(30) Danquah, M.; Li, F.; Duke, C. B., 3rd; Miller, D. D.; Mahato, R. I. Micellar Delivery of Bicalutamide and Embelin for Treating Prostate Cancer. *Pharm. Res.* **2009**, *26*, 2081−2092.

(31) Skrott, Z.; Cvek, B. Diethyldithiocarbamate Complex with Copper: the Mechanism of Action in Cancer Cells. *Mini Rev. Med. Chem.* **2012**, *12*, 1184−1192.

(32) Wang, N.-n.; Wang, L.-H.; Li, Y.; Fu, S.-Y.; Xue, X.; Jia, L.-N.; Yuan, X.-Z.; Wang, Y.-T.; Tang, X.; Yang, J.-Y.; Wu, C.-F. Targeting ALDH2 with Disulfiram/Copper Reverses the Resistance of Cancer Cells to Microtubule Inhibitors. *Exp. Cell Res.* **2018**, *362*, 72−82.

(33) Denoyer, D.; Masaldan, S.; La Fontaine, S.; Cater, M. A. Targeting Copper in Cancer Therapy: "Copper That Cancer". *Metallomics* **2015**, *7*, 1459−1476.

(34) Hoyer-Hansen, M.; Jaattela, M. Connecting Endoplasmic Reticulum Stress to Autophagy by Unfolded Protein Response and Calcium. *Cell Death Differ.* **2007**, *14*, 1576−1582.



DOI: 10.1021/acsami.8b14940
ACS Appl. Mater. Interfaces XXXX, XXX, XXX−XXX

(35) Yang, Y.; Zhang, K.; Wang, Y.; Li, M.; Sun, X.; Liang, Z.; Wang, L.; Chen, L.; Yang, H.; Zhu, L. Disulfiram Chelated with Copper Promotes Apoptosis in Human Breast Cancer Cells by Impairing the Mitochondria Functions. *Scanning* **2016**, *38*, 825−836.
(36) Breckenridge, D. G.; Germain, M.; Mathai, J. P.; Nguyen, M.; Shore, G. C. Regulation of Apoptosis by Endoplasmic Reticulum Pathways. *Oncogene* **2003**, *22*, 8608−8618.
(37) Nobel, C. S. I.; Kimland, M.; Nicholson, D. W.; Orrenius, S.; Slater, A. F. G. Disulfiram is a Potent Inhibitor of Proteases of the Caspase Family. *Chem. Res. Toxicol.* **1997**, *10*, 1319−1324.
(38) Tardito, S.; Bassanetti, I.; Bignardi, C.; Elviri, L.; Tegoni, M.; Mucchino, C.; Bussolati, O.; Franchi-Gazzola, R.; Marchiò, L. Copper Binding Agents Acting as Copper Ionophores Lead to Caspase Inhibition and Paraptotic Cell Death in Human Cancer Cells. *J. Am. Chem. Soc.* **2011**, *133*, 6235−6242.
(39) Zhou, Y.; Huang, F.; Yang, Y.; Wang, P.; Zhang, Z.; Tang, Y.; Shen, Y.; Wang, K. Paraptosis-Inducing Nanomedicine Overcomes Cancer Drug Resistance for a Potent Cancer Therapy. *Small* **2018**, *14*, 1702446.
(40) Chen, X.; Zhang, X.; Chen, J.; Yang, Q.; Yang, L.; Xu, D.; Zhang, P.; Wang, X.; Liu, J. Hinokitiol Copper Complex Inhibits Proteasomal Deubiquitination and Induces Paraptosis-like Cell Death in Human Cancer Cells. *Eur. J. Pharmacol.* **2017**, *815*, 147−155.
(41) Barilli, A.; Atzeri, C.; Bassanetti, I.; Ingoglia, F.; Dall'Asta, V.; Bussolati, O.; Maffini, M.; Mucchino, C.; Marchiò, L. Oxidative Stress Induced by Copper and Iron Complexes with 8-hydroxyquinoline Derivatives Causes Paraptotic Death of HeLa Cancer Cells. *Mol. Pharm.* **2014**, *11*, 1151−1163.


DOI: 10.1021/acsami.8b14940
*ACS Appl. Mater. Interfaces* XXXX, XXX, XXX−XXX

**Supporting Information**

# Disulfiram Copper Nanoparticles Prepared with a Stabilized Metal Ion Ligand Complex (SMILE) Method for Treating Drug-Resistant Prostate Cancers

*Wu Chen[1], Wen Yang[2], Pengyu Chen[2], Yongzhuo Huang[3,*], Feng Li[1,*]*

1. Department of Drug Discovery and Development, Harrison School of Pharmacy, Auburn University, Auburn, AL 36849 USA
2. Department of Material Engineering, Auburn University, Auburn, AL 36849 USA
3. Shanghai Institute of Materia Medica, Chinese Academy of Sciences, Shanghai 201203, China

**Corresponding authors:**

**Feng Li, PhD**

720 S. Donahue Dr. Auburn, AL 36849, USA

Tel:334-844-7406
Email: FZL0023@auburn.edu

**Yongzhuo Huang, PhD**

501 Haike Rd, Shanghai 201203, China

Tel: +86-21-2023-1981

Email: yzhuang@simm.ac.cn

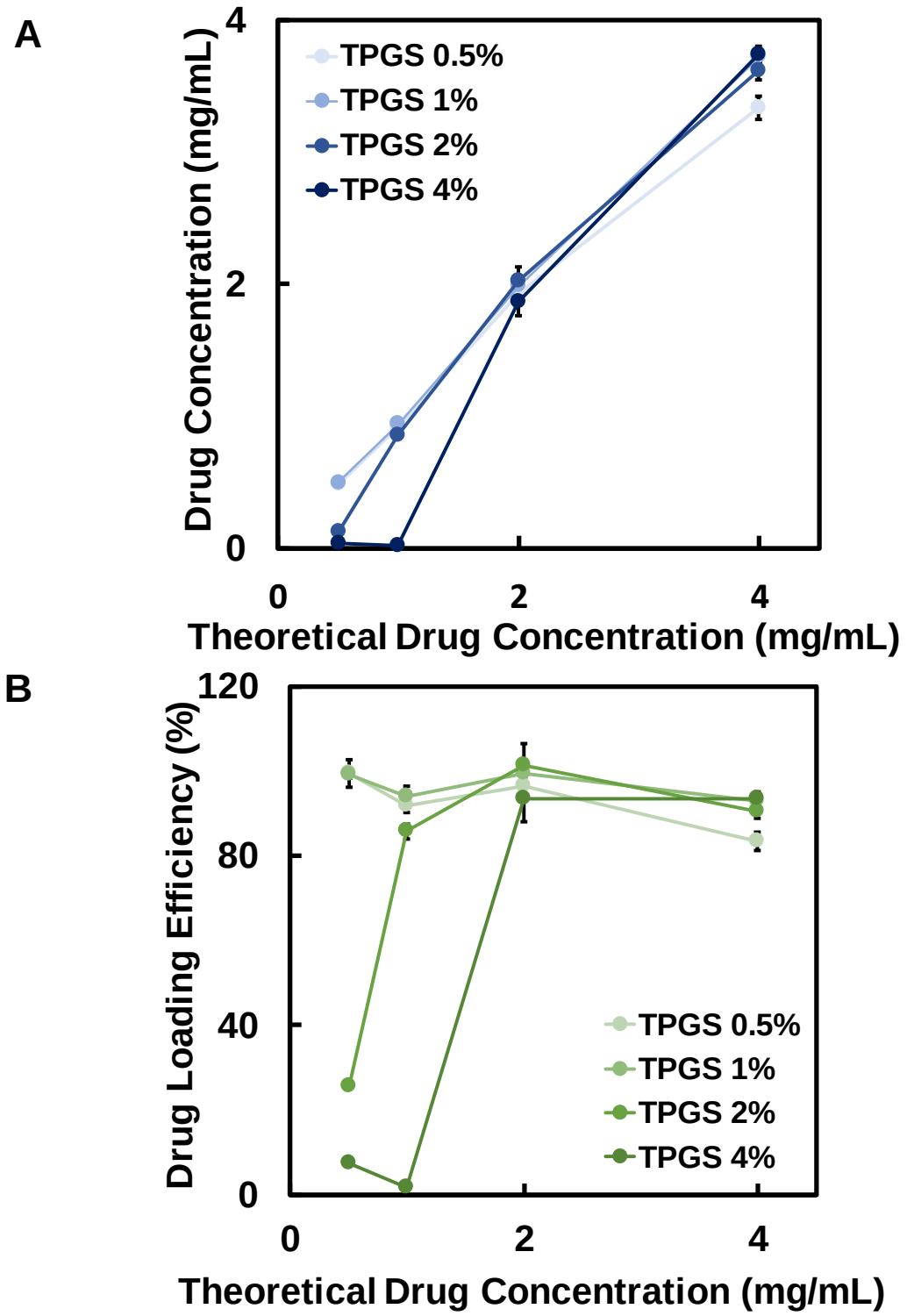


**Figure S1**. Effects Theoretical Drug Concentration and TPGS Concentration on Actually $Cu(DDC)_2$ Drug Concentration (**A**) and Drug Loading Efficiency (**B**). Results are the mean ± SD (n = 3).

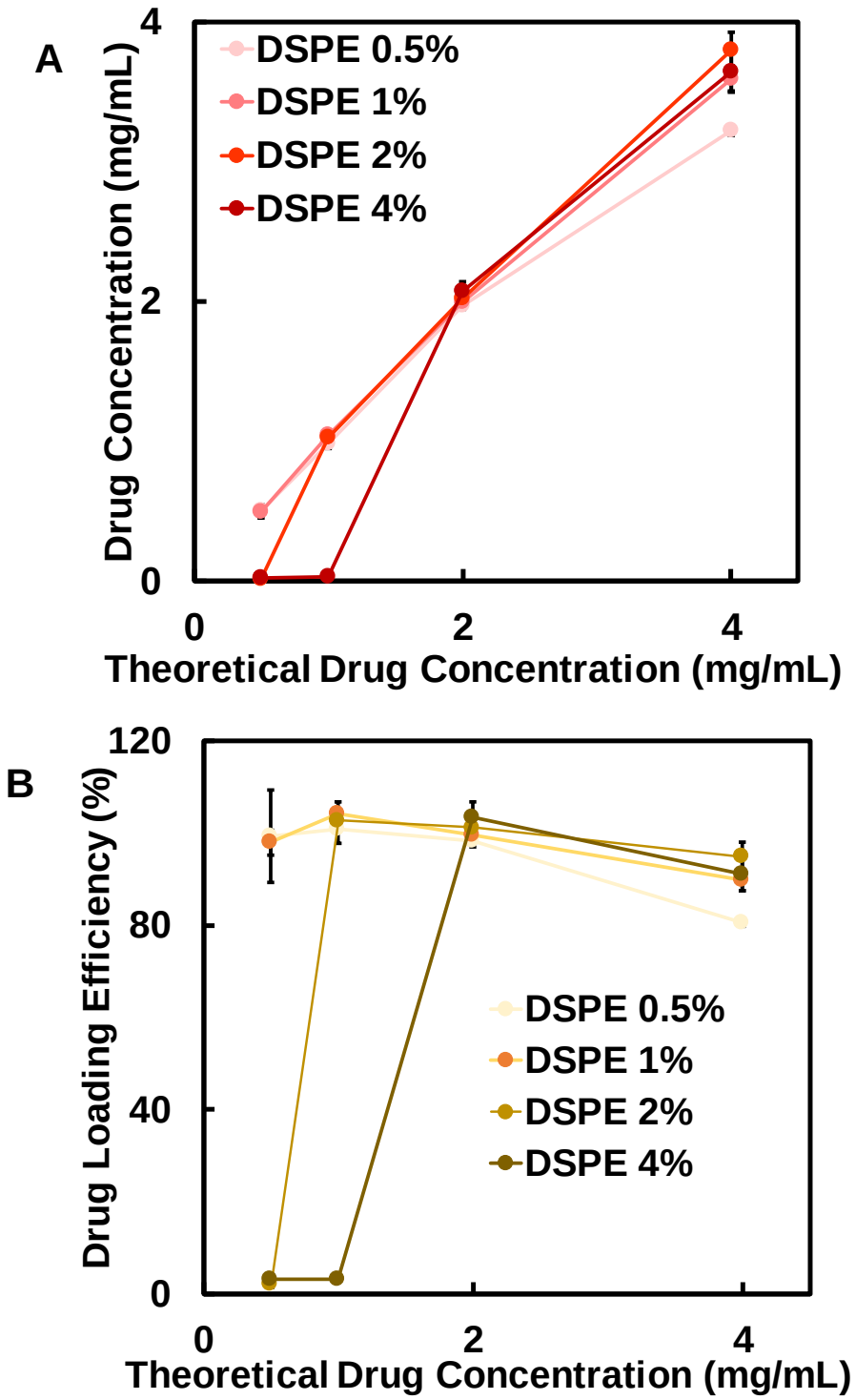


**Figure S2**. Effects theoretical drug concentration and DSPE-PEG concentration on actually $Cu(DDC)_2$ drug concentration (**A**) and drug loading efficiency (**B**). Results are the mean ± SD (n = 3).

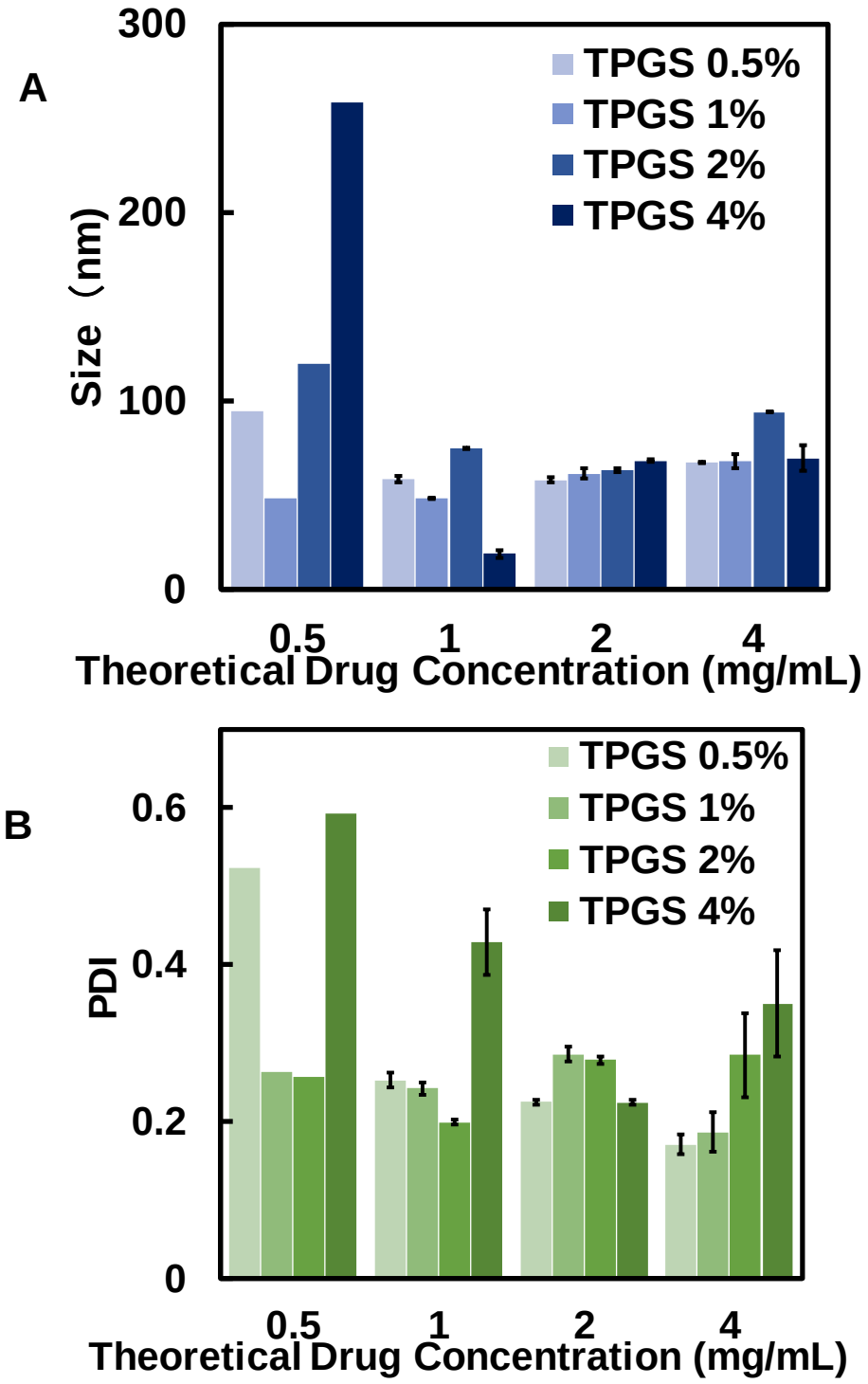


**Figure S3**. Effects theoretical drug concentration and TPGS concentration on NP particle size (**A**) and polydispersity index (PdI)(**B**). Results are the mean ± SD (n = 3).

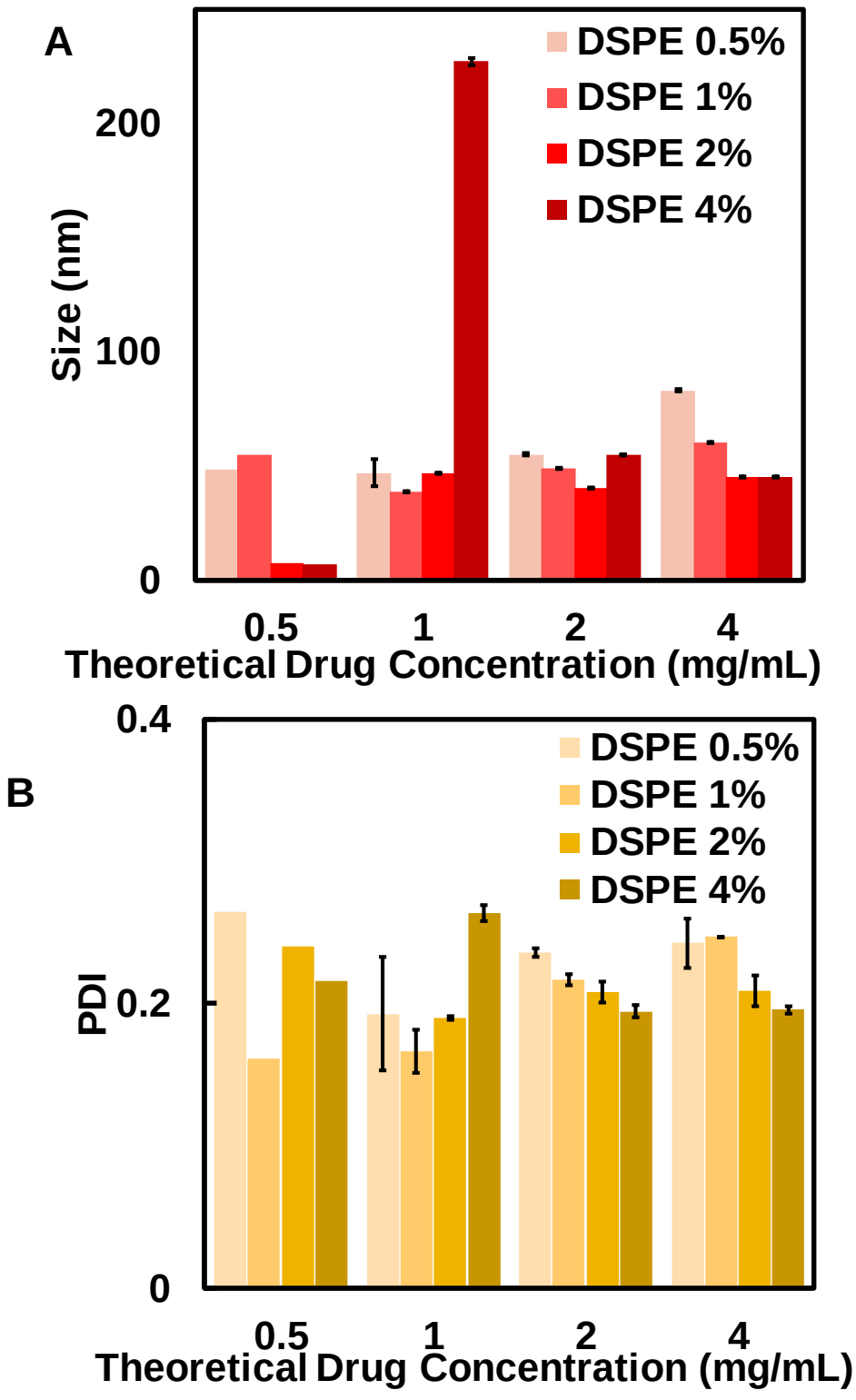


**Figure S4**. Effects theoretical drug concentration and DSPE-PEG concentration on NP particle size (**A**) and polydispersity index (PdI)(**B**). Results are the mean ± SD (n = 3).

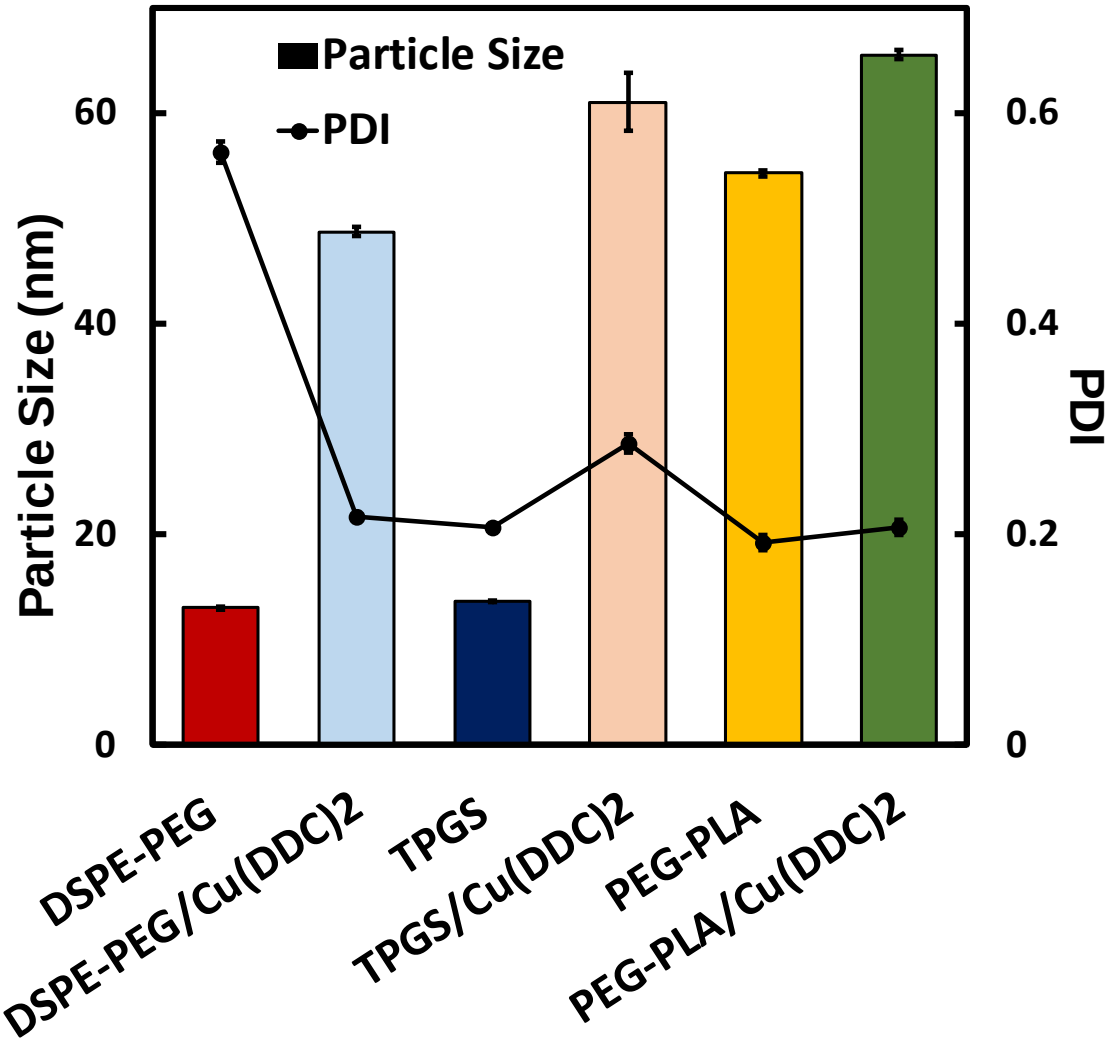


**Figure S5**. Particle size of 2mg/mL $Cu(DDC)_2$ NPs and corresponding stabilizers without $Cu(DDC)_2$. Polymer concentrations were 1%. Results are the mean ± SD (n = 3).

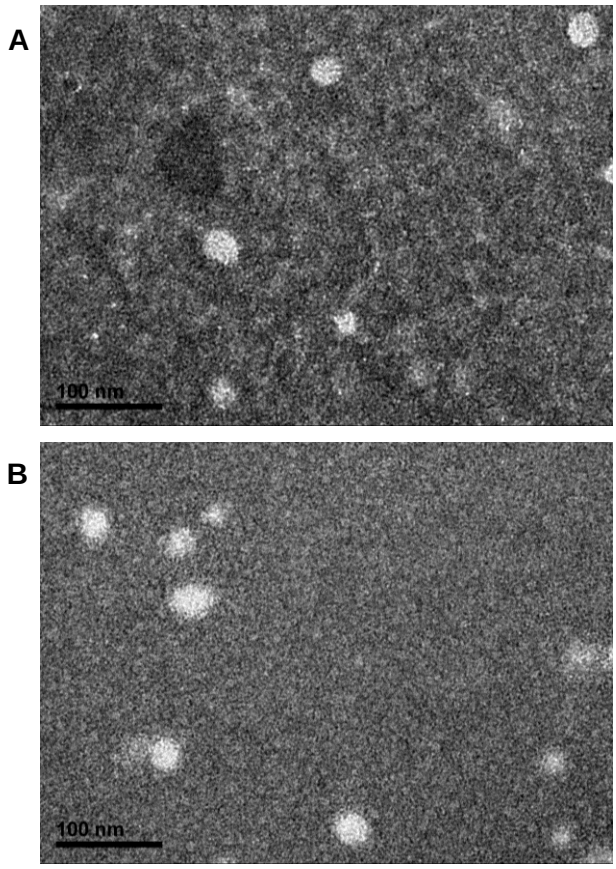


**Figure S6**. Transmission electron microscopy (TEM) of (A) PEG-PLA micelles and (B) PEG-PLA/Cu(DDC)$_2$ NPs. Samples were stained with stained with 1% uranyl acetate.

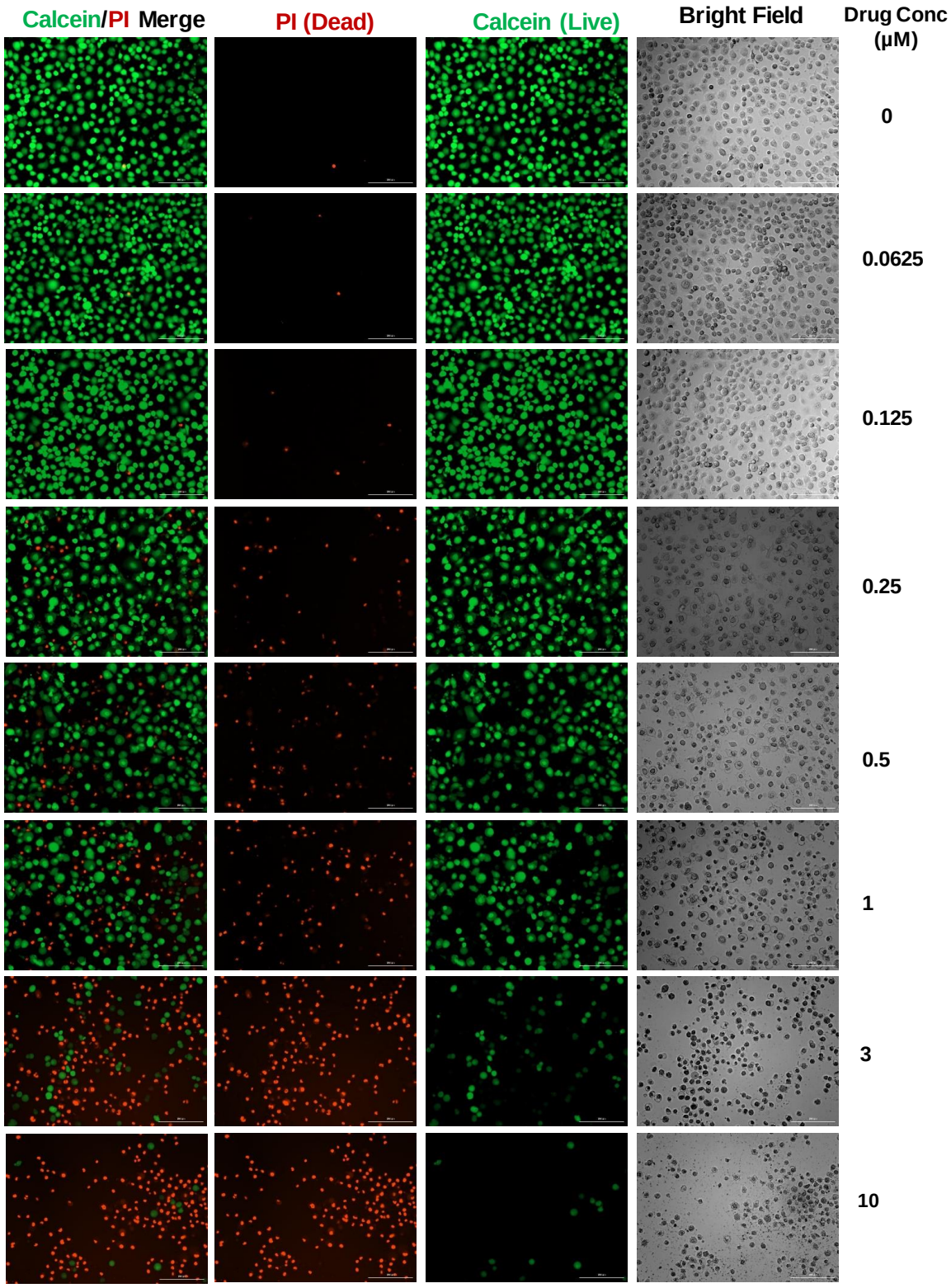


**Figure S7.** Calein AM/PI Staining of DU145-TXR cells treated with $Cu(DDC)_2$ NPs.

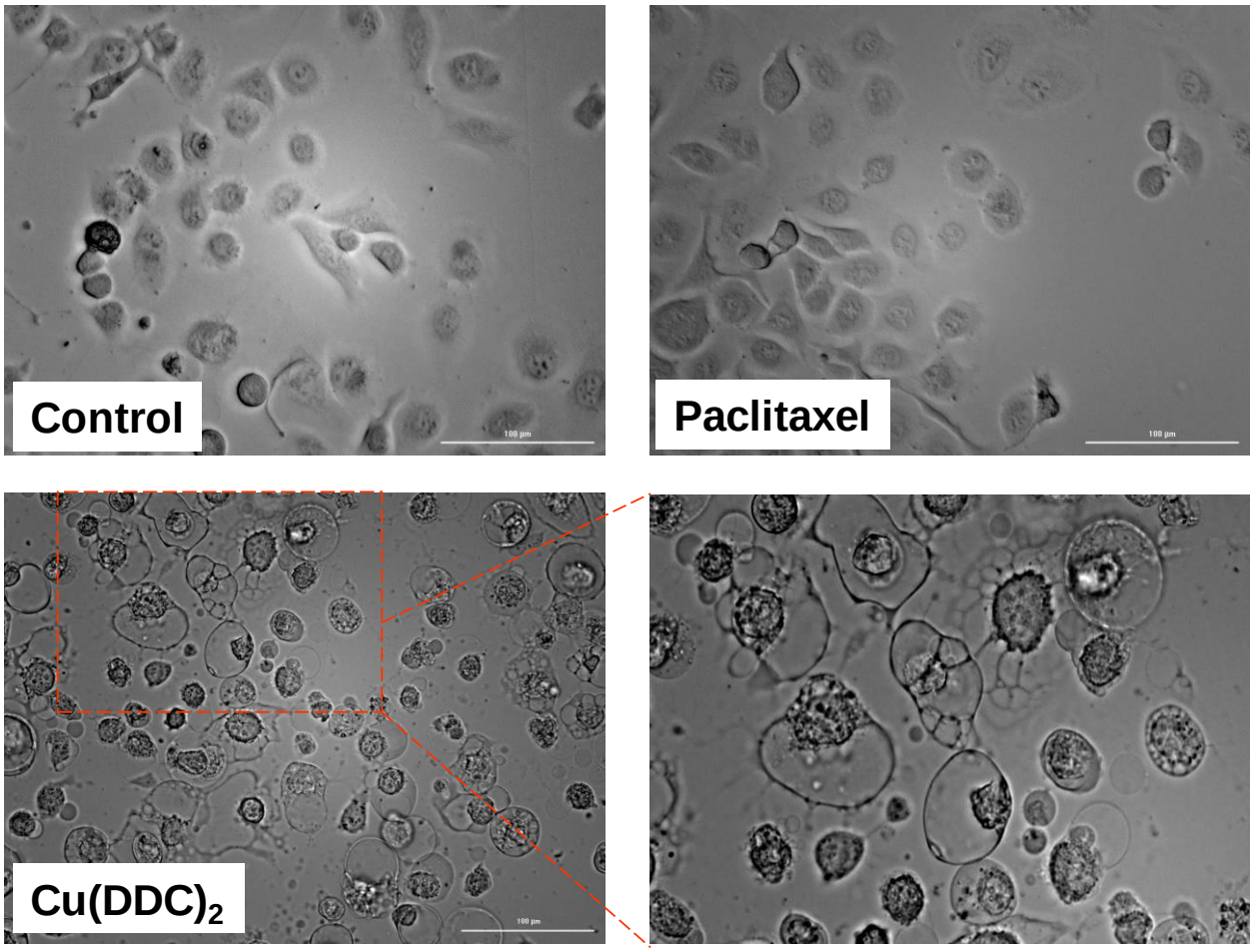


**Figure S8**. Morphology of DU145-TXR cells treated with $Cu(DDC)_2$ NPs (0.5 µM), Paclitaxel (0.5 µM), and blank PEG-PLA for 24 hours.

**Control**

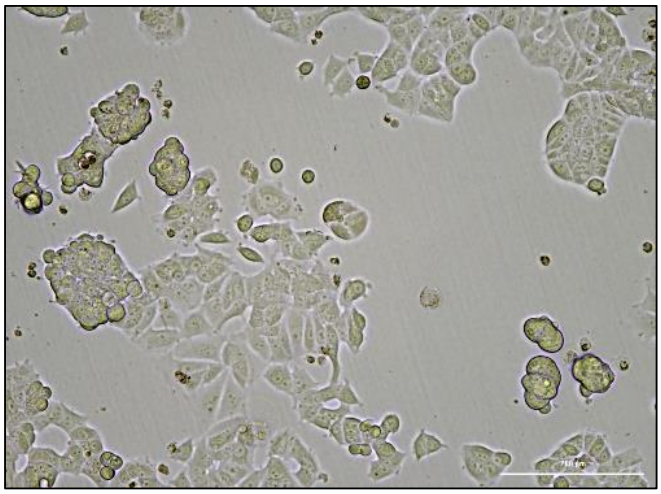

**$Cu(DDC)_2$ NPs 0.5 µM**

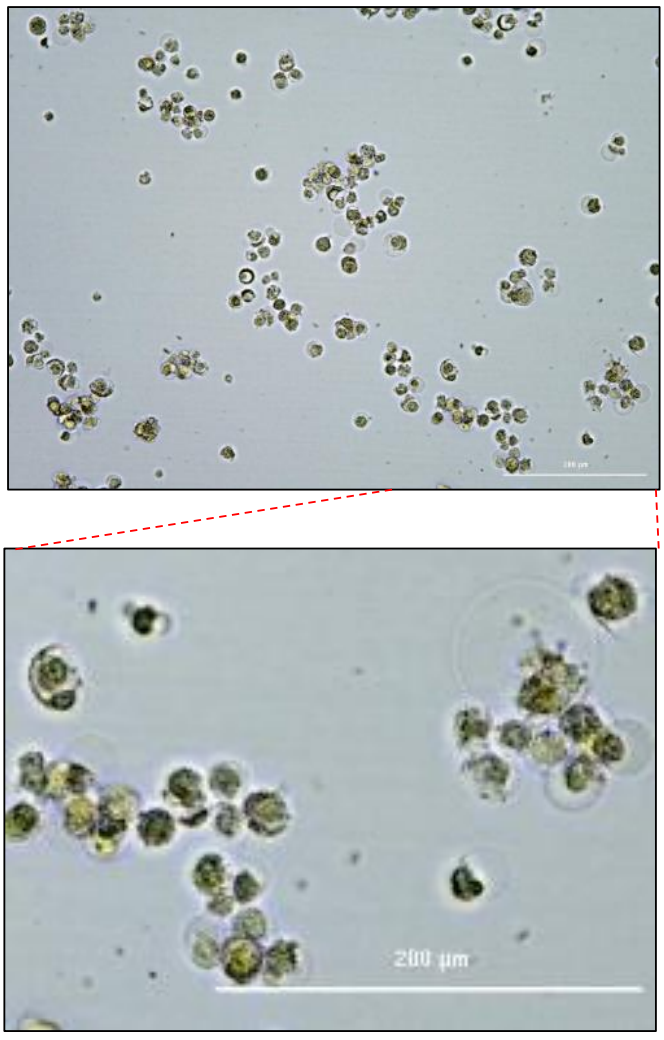


**Figure S9:** Morphology of MCF-7 Cells Treated with 0.5 µM DSPE-PEG/$Cu(DDC)_2$ NPs for 72 hours. Control was DSPE-PEG without $Cu(DDC)_2$.

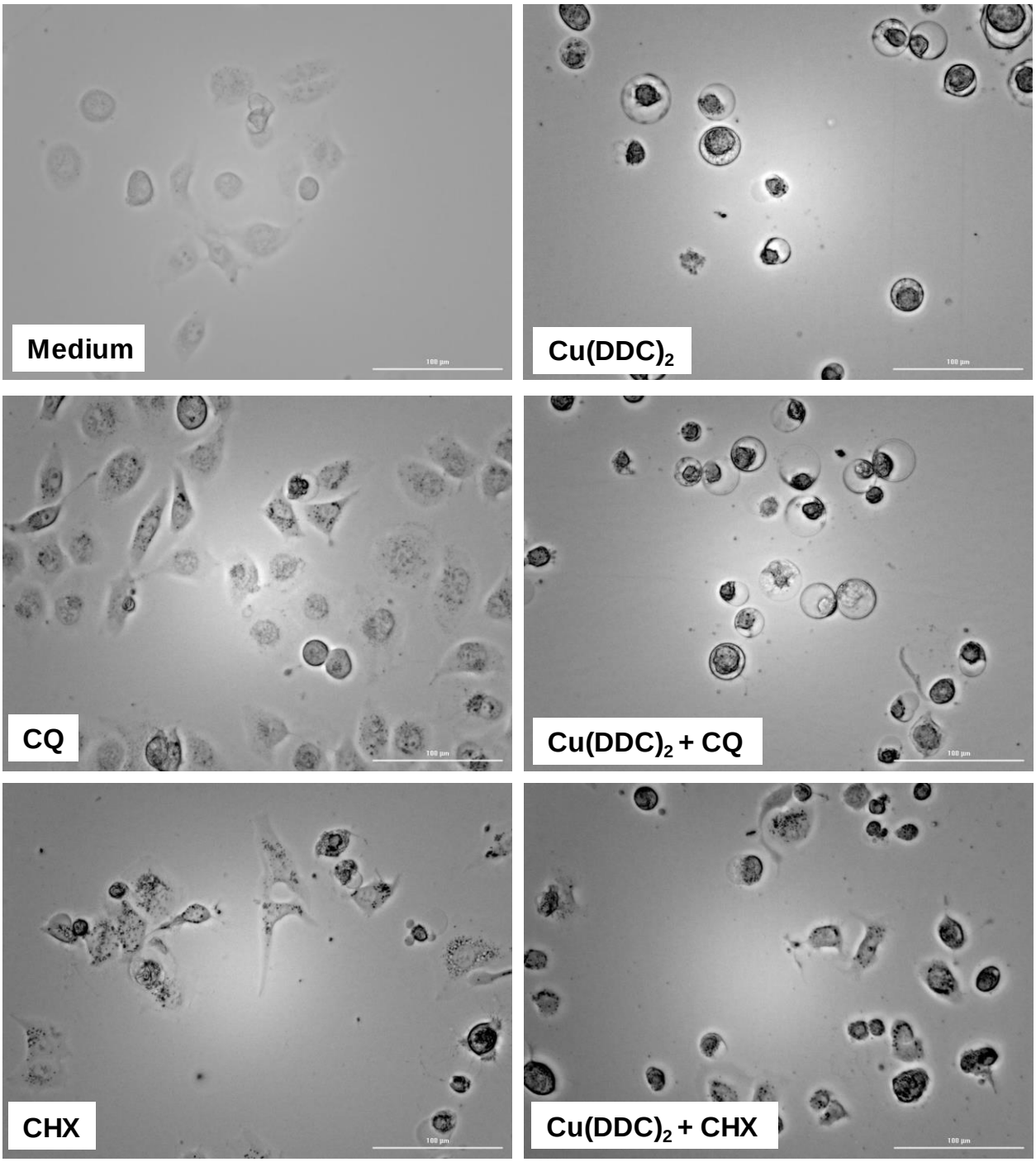


**Figure S10**. Morphology of Du145-TXR cells treated with $Cu(DDC)_2$ NPs (0.5 μM) alone and in combination with cycloheximide (CHX, 20 μM) or chloroquine (CQ 20 μM) for 24 hours.